Molecular Dynamics of a Liquid Crystal by Deuterium NMR Study

BY

XIAODONG SHEN

A Thesis

Submitted to the Faculty of Graduate Studies

in Partial Fulfillment of the Requirements

for the Degree of

MASTER OF SCIENCE

Department of Physics

University of Manitoba

Winnipeg, Manitoba

ISBN 0-315-98982-3

Name Shen Xiaodong

Dissertation Abstracts International is arranged by broad, general subject categories. Please select the one subject which most nearly describes the content of your dissertation. Enter the corresponding four-digit code in the spaces provided.

Molecular
SUBJECT TERM

0609
SUBJECT CODE

U·M·I

Subject Categories

THE HUMANITIES AND SOCIAL SCIENCES

COMMUNICATIONS AND THE ARTS
Architecture 0729
Art History 0377
Cinema 0900
Dance 0378
Fine Arts 0357
Information Science 0723
Journalism 0391
Library Science 0399
Mass Communications 0708
Music 0413
Speech Communication 0459
Theater 0465

EDUCATION
General 0515
Administration 0514
Adult and Continuing 0516
Agricultural 0517
Art 0273
Bilingual and Multicultural 0282
Business 0688
Community College 0275
Curriculum and Instruction 0727
Early Childhood 0518
Elementary 0524
Finance 0277
Guidance and Counseling 0519
Health 0680
Higher 0745
History of 0520
Home Economics 0278
Industrial 0521
Language and Literature 0279
Mathematics 0280
Music 0522
Philosophy of 0998
Physical 0523
Psychology 0525
Reading 0535
Religious 0527
Sciences 0714
Secondary 0533
Social Sciences 0534
Sociology of 0340
Special 0529
Teacher Training 0530
Technology 0710
Tests and Measurements 0288
Vocational 0747

LANGUAGE, LITERATURE AND LINGUISTICS
Language
- General 0679
- Ancient 0289
- Linguistics 0290
- Modern 0291

Literature
- General 0401
- Classical 0294
- Comparative 0295
- Medieval 0297
- Modern 0298
- African 0316
- American 0591
- Asian 0305
- Canadian (English) 0352
- Canadian (French) 0355
- English 0593
- Germanic 0311
- Latin American 0312
- Middle Eastern 0315
- Romance 0313
- Slavic and East European 0314

PHILOSOPHY, RELIGION AND THEOLOGY
Philosophy 0422
Religion
- General 0318
- Biblical Studies 0321
- Clergy 0319
- History of 0320
- Philosophy of 0322

Theology 0469

SOCIAL SCIENCES
American Studies 0323
Anthropology
- Archaeology 0324
- Cultural 0326
- Physical 0327

Business Administration
- General 0310
- Accounting 0272
- Banking 0770
- Management 0454
- Marketing 0338

Canadian Studies 0385
Economics
- General 0501
- Agricultural 0503
- Commerce-Business 0505
- Finance 0508
- History 0509
- Labor 0510
- Theory 0511

Folklore 0358
Geography 0366
Gerontology 0351
History
- General 0578
- Ancient 0579
- Medieval 0581
- Modern 0582
- Black 0328
- African 0331
- Asia, Australia and Oceania 0332
- Canadian 0334
- European 0335
- Latin American 0336
- Middle Eastern 0333
- United States 0337

History of Science 0585
Law 0398
Political Science
- General 0615
- International Law and Relations 0616
- Public Administration 0617

Recreation 0814
Social Work 0452
Sociology
- General 0626
- Criminology and Penology 0627
- Demography 0938
- Ethnic and Racial Studies 0631
- Individual and Family Studies 0628
- Industrial and Labor Relations 0629
- Public and Social Welfare 0630
- Social Structure and Development 0700
- Theory and Methods 0344

Transportation 0709
Urban and Regional Planning 0999
Women's Studies 0453

THE SCIENCES AND ENGINEERING

BIOLOGICAL SCIENCES
Agriculture
- General 0473
- Agronomy 0285
- Animal Culture and Nutrition 0475
- Animal Pathology 0476
- Food Science and Technology 0359
- Forestry and Wildlife 0478
- Plant Culture 0479
- Plant Pathology 0480
- Plant Physiology 0817
- Range Management 0777
- Wood Technology 0746

Biology
- General 0306
- Anatomy 0287
- Biostatistics 0308
- Botany 0309
- Cell 0379
- Ecology 0329
- Entomology 0353
- Genetics 0369
- Limnology 0793
- Microbiology 0410
- Molecular 0307
- Neuroscience 0317
- Oceanography 0416
- Physiology 0433
- Radiation 0821
- Veterinary Science 0778
- Zoology 0472

Biophysics
- General 0786
- Medical 0760

EARTH SCIENCES
Biogeochemistry 0425
Geochemistry 0996
Geodesy 0370
Geology 0372
Geophysics 0373
Hydrology 0388
Mineralogy 0411
Paleobotany 0345
Paleoecology 0426
Paleontology 0418
Paleozoology 0985
Palynology 0427
Physical Geography 0368
Physical Oceanography 0415

HEALTH AND ENVIRONMENTAL SCIENCES
Environmental Sciences 0768
Health Sciences
- General 0566
- Audiology 0300
- Chemotherapy 0992
- Dentistry 0567
- Education 0350
- Hospital Management 0769
- Human Development 0758
- Immunology 0982
- Medicine and Surgery 0564
- Mental Health 0347
- Nursing 0569
- Nutrition 0570
- Obstetrics and Gynecology 0380
- Occupational Health and Therapy 0354
- Ophthalmology 0381
- Pathology 0571
- Pharmacology 0419
- Pharmacy 0572
- Physical Therapy 0382
- Public Health 0573
- Radiology 0574
- Recreation 0575
- Speech Pathology 0460
- Toxicology 0383

Home Economics 0386

PHYSICAL SCIENCES
Pure Sciences
Chemistry
- General 0485
- Agricultural 0749
- Analytical 0486
- Biochemistry 0487
- Inorganic 0488
- Nuclear 0738
- Organic 0490
- Pharmaceutical 0491
- Physical 0494
- Polymer 0495
- Radiation 0754

Mathematics 0405
Physics
- General 0605
- Acoustics 0986
- Astronomy and Astrophysics 0606
- Atmospheric Science 0608
- Atomic 0748
- Electronics and Electricity 0607
- Elementary Particles and High Energy 0798
- Fluid and Plasma 0759
- Molecular 0609
- Nuclear 0610
- Optics 0752
- Radiation 0756
- Solid State 0611

Statistics 0463

Applied Sciences
Applied Mechanics 0346
Computer Science 0984
Engineering
- General 0537
- Aerospace 0538
- Agricultural 0539
- Automotive 0540
- Biomedical 0541
- Chemical 0542
- Civil 0543
- Electronics and Electrical 0544
- Heat and Thermodynamics 0348
- Hydraulic 0545
- Industrial 0546
- Marine 0547
- Materials Science 0794
- Mechanical 0548
- Metallurgy 0743
- Mining 0551
- Nuclear 0552
- Packaging 0549
- Petroleum 0765
- Sanitary and Municipal 0554
- System Science 0790

Geotechnology 0428
Operations Research 0796
Plastics Technology 0795
Textile Technology 0994

PSYCHOLOGY
General 0621
Behavioral 0384
Clinical 0622
Developmental 0620
Experimental 0623
Industrial 0624
Personality 0625
Physiological 0989
Psychobiology 0349
Psychometrics 0632
Social 0451

MOLECULAR DYNAMICS OF A LIQUID CRYSTAL BY DEUTERIUM NMR STUDY

BY

XIAODONG SHEN

A Thesis submitted to the Faculty of Graduate Studies of the University of Manitoba in partial fulfillment of the requirements of the degree of

MASTER OF SCIENCE

To my Parents

Abstract

Deuterium nuclear magnetic resonance (NMR) spectroscopy was used to explore molecular motions in the mesophases of $4-n-$pentyloxybenzylidene$-d_1-4'-$heptylaniline and $4-n-$pentyloxybenzylidene$-4'-$heptylaniline$-2,3,5,6-d_4$. The Zeeman and quadrupolar spin$-$lattice relaxation times were measured as a function of temperature at 15.3 MHz and 46 MHz using a broadband multiple$-$pulse sequence. We found that quite different motional mechanisms are involved between the "disordered" liquid-like phases (nematic, smectic A and C phases) and the "ordered" solid-like phases (smectic B and G phases).

Firstly, in the "disordered" liquid-like phases, the motional spectral densities can only be interpreted by invoking director fluctuations and molecular reorientation as relaxation mechanisms for the deuteron spins at the methine and ring sites. The contribution from director fluctuations is more or less the same in the nematic, smectic A and C phases of 5O.7. We compared Nordio's model and the third rate model of molecular reorientation and found that the third rate model is more appropriate in the present study. Rotational diffusion constants were determined as a function of temperature in these mesophases.

Secondly, in the "ordered" solid-like phases, the model of restricted libration of molecular rotation about the long z_M axis is needed to explain the spectral density data. This biased motional model is a simple extension of the third rate model. The observed temperature, site and frequency dependences of the relaxation data

can be fitted well in the smectic B and G phases. The biaxial terms in the spectral densities are found to vanish as long as the director is aligned with the external field. The lack of discontinuities at uniaxial–biaxial phase transitions is predicted by the appropriate theory.

Acknowldgments

I thank my supervisor, Professor R.Y. Dong, for his guidance, enthusiasm and support throughout my years as a graduate student. I learned a great deal of NMR and liquid crystal from him. Also I would like to thank him for the countless hours he spent in helping me in the lab, answering my questions, proof reading this paper as well as solving problems that related to me being an international student. A special thank goes to Mr. Norm Finlay for his great help in fixing experimental apparatus and solving many practical problems. I would also like to thank Mr. D. Bramadat for his technical assistance during the earlier part of this work.

I am grateful to the Natural Science and Engineering Research for financial support and to Brandon University for using its facilities.

I would like to thank the members of my advisory committee; Professors J.H. Page and Ted Schaefer. I also thank Professor G.C. Tabisz, Ms. Shirley Bergen and Ms. X.J. Wang for their great help.

I have enjoyed the companion of the members on the 2nd floor of Brodie Building, Brandon University. There are many and I thank them all, in particular Dr. G.M. Richards for beneficial discussions and Professor R.A. Giles for reason I am sure he is well aware.

A special thanks is extended to my family, my parents Y.Z. Shen and Y.Q. Chen and my wife Y. He, for all their understanding, encouragement and support over the years. Finally, I would like to thank Mr. Don Coultes, Mr. T.L. Zhou, Ms.

Y.X. Ge and Mr. G.Q. Yang for their friendships and kindness.

Table of Contents

List of Tables

List of Figures

Chapter 1

Introduction

Liquid crystals are composed of flexible organic molecules and are capable of forming different ordered structures in their mesophases. Nuclear magnetic resonance (NMR) is a spectroscopic technique which can provide information on the molecular dynamics of liquid crystals [1]. Mesogenic molecules usually contain a rigid core and one or more pendant alkyl chains. Recently internal dynamics of mesogenic molecules have attracted much efforts; both experimental and theoretical studies have been carried out. Experimentally, deuterium NMR can be used to probe relations among the NMR observables.

The spectroscopic timescale for ^{2}H NMR, $\tau_s \approx 3 \times 10^{-6}$s, is long enough to render appreciable motional–averaging due to molecular motions. Thus NMR occupies a unique place among spectroscopic techniques. The slow motions, which have correlation time $\tau_c \gg \tau_s$, have negligible influence on the NMR spectrum. The fast motions, i.e. $\tau_c \ll \tau_s$, have a large influence on the spectrum due to motional–averaging of spin interactions over fast motions. The site specificity of deuterons is often evident in the ^{2}H NMR spectrum, and the thermally driven molecular motion can be studied by spin relaxation time measurements.

1.1 Basic NMR

The application of a magnetic field $\vec{H}_0$ produces an interaction energy of

$$\mathcal{H}_Z = -\vec{\mu} \bullet \vec{H}_0 = -\gamma\hbar\vec{I} \bullet \vec{H}_0 = -\gamma\hbar H_0 I_z \tag{1}$$

where $\vec{\mu}$ is the nuclear magnetic moment, γ is the gyromagnetic ratio , $\vec{I}$ is the nuclear spin operator and the field $\vec{H}_0$ is taken along the Z_L direction of a laboratory frame. The effect of an alternating magnetic field $H_x(t) = H_{x0}\cos\omega t$ is analyzed by decomposing it into two rotating components, each of amplitude $H_1 = H_{x0}/2$ and one rotating clockwise while the other counterclockwise [2,3].

$$\begin{aligned} \vec{H}_R &= H_1(\hat{\imath}\cos\omega t + \hat{\jmath}\sin\omega t) \\ \vec{H}_L &= H_1(\hat{\imath}\cos\omega t - \hat{\jmath}\sin\omega t) \end{aligned} \tag{2}$$

The $\vec{H}_R$ and $\vec{H}_L$ differ just by ω changing sign to $-\omega$. Without loss in generality, we use $\vec{\omega} = \omega_z\hat{k}$ to write

$$\vec{H}_1(t) = H_1(\hat{\imath}\cos\omega_z t + \hat{\jmath}\sin\omega_z t) \tag{3}$$

Since $\vec{\mu} = \gamma\vec{p}$, where $\vec{p}$ is the angular momentum of the spinning nucleus, the motion of the magnetic moment in a magnetic field satisfies the following equation:

$$\frac{d\vec{\mu}}{dt} = \gamma\frac{d\vec{p}}{dt} = \gamma\vec{\mu} \times \vec{H} \tag{4}$$

The total macroscopic magnetization, $\vec{M}$, is the vector sum of the magnetic moments. Thus, the vectorial sum of eq. (4) produces the equation of motion

$$\frac{d\vec{M}}{dt} = \gamma\vec{M} \times \vec{H} = \vec{M} \times \gamma\left[\vec{H}_0 + \vec{H}_1(t)\right] \tag{5}$$

The time dependence of $\vec{H}_1$ can be eliminated by using a coordinate system $(\hat{i}', \hat{j}', \hat{k}')$ that rotates about the laboratory Z_L-direction at a frequency ω_z. Then both $\vec{H}_1$ and $\vec{H}_0$ will be static in such a coordinate system. The above equation becomes:

$$\frac{d\vec{M}}{dt} = \vec{M} \times \left[\hat{k}'(\omega_z + \gamma H_0) + \hat{i}'\gamma H_1\right] \tag{6}$$

Note that the ω_z term is associated with the derivative of a rotating unit vector. At exact resonance, the alternating field effectively cancels the effect of the static field. Therefore, $\omega_z + \gamma H_0$ approaches zero by setting $\omega_z = -\omega$ and

$$\frac{d\vec{M}}{dt} = \vec{M} \times \gamma \left[\hat{k}'(H_0 - \frac{\omega}{\gamma}) + \hat{i}'H_1\right] = \vec{M} \times \gamma \vec{H}_{eff} \tag{7}$$

$$\vec{H}_{eff} = \hat{k}'(H_0 - \frac{\omega}{\gamma}) + H_1\hat{i}' \tag{8}$$

Equation (7) states that in the rotating frame, the magnetization acts as though it is effectively experiencing a static magnetic field $\vec{H}_{eff}$. The magnetization therefore precesses in a cone of fixed angle about the direction of $\vec{H}_{eff}$ at angular frequency γH_{eff}. Figure 1 shows the situation which at t=0, the magnetization was oriented along the Z_L-direction.

When the resonance condition is fulfilled exactly ($\omega = \gamma H_0$), only $\vec{H}_1$ is left to interact with the magnetization. The magnetization which is initially parallel to $\vec{H}_0$ will then precess in the $y' - z'$ plane of the rotating coordinate system. That is, it will always precess perpendicular to $\vec{H}_1$, with a frequency γH_1. The angle through which $\vec{M}$ rotates in a period of time t_p is given by:

$$\theta = \gamma H_1 t_p \tag{9}$$

1.2 Relaxation

The phenomenon of evolution towards the statistical equilibrium of a macroscopic system is given the name 'relaxation'. From eq. (9), it would seem that once $\vec{M}$ is rotated by an angle θ, $\vec{M}$ could stay at this new position indefinitely. In reality, the spins of nuclei interact with their surroundings. As a result, $\vec{M}$ decays back to its original state. This process is a first order rate process and is characterized by a spin-lattice relaxation time T_1. The nuclear spins will also come to equilibrium with each other, which is characterized by a spin-spin relaxation time T_2.

When a static field is applied along the Z_L axis, the longitudinal magnetization M_z has an equilibrium value M_0, whereas the transverse components M_x and M_y vanish at thermal equilibrium. Starting from a non-equilibrium state, the evolution of M_z towards M_0 modifies the energy of the spin system through exchange of energy with the lattice, whereas the decrease in transverse magnetization components does not produce such an exchange of energy and is the effect of spin-spin interactions among nuclear spins. Motions that contribute to T_1 also contribute to T_2 so that $T_2 \leq T_1$ is always satisfied.

Assuming that nuclear spins have been aligned so that N_α of them are in the α state and N_β in the β state, the population difference $n(= N_\alpha - N_\beta)$ decays exponentially to equilibrium because of the spin-lattice relaxation, according to

$$\frac{dn}{dt} = -\frac{n - n_0}{T_1} \tag{10}$$

The presence of n_0 is due to the static field $\vec{H}_0$ in the Z_L direction. The M_z is proportional to n and obeys

$$\frac{dM_z}{dt} = -\frac{M_z - M_0}{T_1} \tag{11}$$

Similarly, the transverse components M_x and M_y of the magnetization vector will decay exponentially to zero, but with a spin-spin (transverse) relaxation time T_2

$$\frac{dM_x}{dt} = -\frac{M_x}{T_2} \quad ; \quad \frac{dM_y}{dt} = -\frac{M_y}{T_2} \tag{12}$$

Including the Larmor precessing of $\vec{M}$ in the field $\vec{H}$, we have

$$\begin{aligned} \frac{dM_z}{dt} &= \gamma(\vec{M} \times \vec{H})_z - \frac{M_z - M_0}{T_1} \\ \frac{dM_x}{dt} &= \gamma(\vec{M} \times \vec{H})_x - \frac{M_x}{T_2} \\ \frac{dM_y}{dt} &= \gamma(\vec{M} \times \vec{H})_y - \frac{M_y}{T_2} \end{aligned} \tag{13}$$

Since $\vec{H}$ is the sum of static field $\vec{H}_0$ and alternating field $\vec{H}_1$ (eq. (3)), the above Bloch's equation becomes

$$\frac{d\vec{M}}{dt} = \gamma(\vec{M} \times \vec{H}_0) + \gamma(\vec{M} \times \vec{H}_1) - \frac{(\hat{\imath}M_x + \hat{\jmath}M_y)}{T_2} - \frac{\hat{k}(M_z - M_0)}{T_1} \tag{14}$$

1.3 Quadrupole Effect

For spin>1/2 nuclei, there are electrical effects on the energy due to orientation of the nucleus in the external field. A simple example is a cigar-shaped nucleus in the field of four charges (Fig. 2), two of which are +q charges on the x-axis and the other two are -q charges on the y-axis. The configuration (b) in which the longer

ends are close to the negative charges corresponds to a lower energy.

The quadrupole Hamiltonian $\mathcal{H}_Q$ arises from an electrostatic interaction of the nuclear quadrupole moment ($Q_{\alpha\beta}$) with the external electric field gradient (efg), $V_{\alpha\beta}(=\nabla\vec{E})$ at the position of the nucleus. $V_{\alpha\beta}$ and $Q_{\alpha\beta}$ are defined as

$$\begin{aligned} Q_{\alpha\beta} &= e\sum_{\kappa(protons)}(3x_{\alpha\kappa}x_{\beta\kappa}-\delta_{\alpha\beta}r_\kappa^2) \\ V_{\alpha\beta} &= \left(\frac{\partial^2 V}{\partial x_\alpha \partial x_\beta}\right)_{nuclei} \end{aligned} \tag{15}$$

Thus, a quadrupole Hamiltonian $\mathcal{H}_Q$ is given by [2]

$$\mathcal{H}_Q = \frac{1}{6}\sum_{\alpha,\beta}V_{\alpha\beta}Q_{\alpha\beta} \tag{16}$$

Since the external field is sourceless at the nuclear position, V must satisfy the Laplace's equation, which gives $V_{xx}+V_{yy}+V_{zz}=0$ in any (x,y,z) coordinate system. Using Clebsch-Gordan coefficients and the Wigner-Eckart theorem, eq. (16) can be rewritten as

$$\begin{aligned} \mathcal{H}_Q &= \frac{eQ}{6I(2I-1)}\sum_{\alpha,\beta}V_{\alpha\beta}\left[\frac{3}{2}(I_\alpha I_\beta+I_\beta I_\alpha)-\delta_{\alpha\beta}I^2\right] \\ eQ &= \left(II\zeta|e\sum_{\kappa}^{protons}(3z_\kappa^2-r_\kappa^2)|II\zeta\right) \end{aligned} \tag{17}$$

In the principal coordinate axis system (PAS) of the efg, all the off-diagonal terms of $V_{\alpha\beta}$ are zero and the quadrupole Hamiltonian is

$$\mathcal{H}_Q = \frac{eQ}{4I(2I-1)}\left[V_{zz}(3I_z^2-I^2)+(V_{xx}-V_{yy})(I_x^2-I_y^2)\right] \tag{18}$$

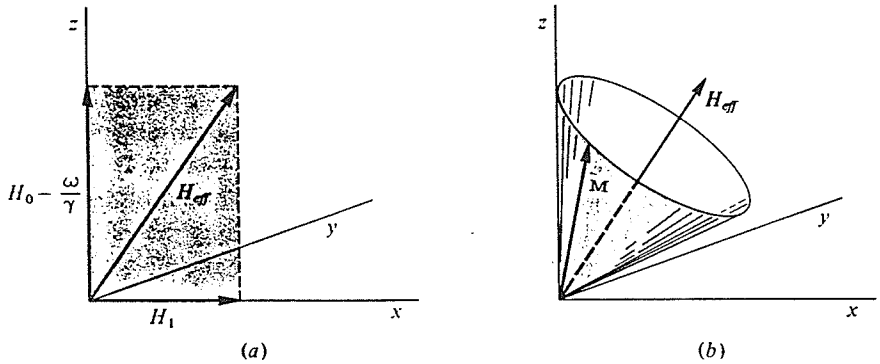

Figure 1 (a) Effective field. (b) Motion of the magnetization in the rotating frame.

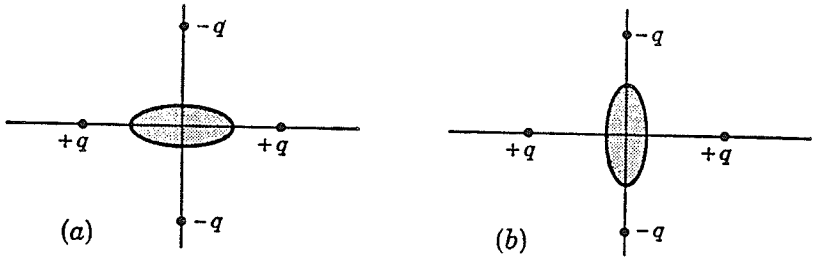

Figure 2 (a) A cigar-shaped nucleus in the field of four charges, $+q$ on the x-axis; $-q$ on the y-axis. The configuration (b) is energetically more favorable because it puts the positive charge of the longer ends of the cigar closer to the negative charges $-q$.

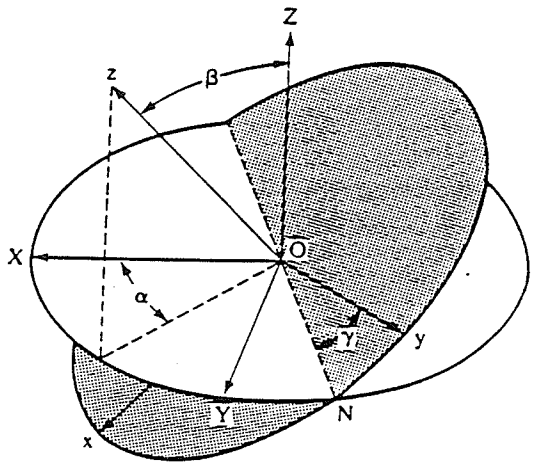

Figure 3 Rotations used in the definition of the Euler angles.

The symbols, η and q, called the *asymmetry parameter* and the *field gradient*, are customarily used and are defined by

$$eq = V_{zz} \quad ; \quad \eta = \frac{V_{xx} - V_{yy}}{V_{zz}} \tag{19}$$

Generally, the efg asymmetry parameter is small for deuterons, ($\eta \leq 0.05$) and can be neglected.

Usually the elements of $V_{\alpha\beta}$ are known in a molecule–fixed coordinate system but the spin operators I_x, I_y and I_z are quantized in the laboratory frame defined by the external magnetic field. Therefore, it is necessary to rotate efg tensor through coordinate transformations using Euler angles (α, β, γ) (Fig. 3). Accordingly $V_{\alpha\beta}$ should be expressed by its irreducible tensor components V_m^2 (m=0,±1,±2).

$$\begin{aligned} V_0^2 &= \sqrt{\frac{3}{2}} V_{zz} \\ V_{\pm 1}^2 &= V_{zx} \pm i V_{zy} = 0 \quad (in\ PAS) \\ V_{\pm 2}^2 &= \frac{1}{2}(V_{xx} - V_{yy}) \pm i V_{xy} = \frac{1}{2}\eta V_{zz} \quad (in\ PAS) \end{aligned} \tag{20}$$

The transformation from one frame to another simply involves the Wigner rotation matrices $D^2_{mm'}(\alpha, \beta, \gamma)$ [2,4]. (See Appendix A for details)

$$V^2_{m'} = \sum_{m=-2}^{2} D^2_{mm'}(\alpha, \beta, \gamma) V^2_m \tag{21}$$

1.4 Liquid Crystal

Liquid Crystalline materials typically involve organic compounds and show a

state of order intermediate between the crystalline lattice and the isotropic liquid. The earlier discoveries of these kinds of materials were near the end of 19th Century (Reinitzer and Lehmann [5]). Today, liquid crystals serve many purposes because of their special mesomorphic properties. Several thousands organic compounds and polymers are known to form liquid crystals. An essential requirement for mesomorphism is that the molecule must be highly anisotropic in its geometry. Liquid crystals may be divided into two categories: thermotropic and lyotropic [6]. Transitions to the intermediate states may be brought about by purely thermal processes (thermotropic mesomorphism) or by the influence of solvents (lyotropic mesomorphism).

1.5 Classification of Mesophases

There are several different phases in thermotropic liquid crystals [6,7]. The structual nature of mesophases is influenced by the molecular shape and therefore depends on whether the liquid crystal is formed by rod-like or disc-like molecules.

In liquid crystals, the molecular axes tend to line up along one direction, called the director $\hat{n}$. The diamagnetic susceptibility tensor $\hat{\chi}$ in a uniaxial medium has two principal components $\chi_{||}$ and $\chi_{\perp}$, which are along and normal to the director, respectively. The diamagnetic susceptibility anisotropy $\Delta\chi(= \chi_{||} - \chi_{\perp})$ is positive for most rod-like molecules, which causes the director to be parallel to the external magnetic field; whereas the discotics have negative $\Delta\chi$, resulting in the director being aligned perpendicular to the external magnetic field [1,8].

Nematic Liquid Crystals

The nematic liquid crystal has a high degree of long range orientational order of the molecules, but no long range position order of the centers of mass. Thus it differs from the isotropic liquid in that molecules are spontaneously oriented with their molecular long axes approximately parallel. For almost all the thermotropic nematics known so far, the nematic phase is uniaxial, which means that there exists rotational symmetry around the director $\hat{n}$. The cholesteric phases may be classified as a special type of nematics. Here molecules are chiral, and tend to align somewhat twisted with respect to one another. This causes the director to rotate in space in a helical (twisted) fashion. The distance for a 360° rotation of the director is called the pitch. Since the pitch is of the order of the wavelength of visible light, cholesterics can be very colourful. Apart from the helical structure, the traditional nematics and cholesterics are very similar. As the pitch becomes infinite, the cholesterics turn into the nematics.

Smectic Liquid Crystals

In smectic phases, molecules not only align parallel to each other but have their cores packed into layers. The molecular centers of mass are, on the average, arranged in equidistant planes. These phases have a certain degree of one-dimensional positional order. There exist many types of smectic phases, labelled $S_A, S_B, \ldots, S_I$ [1]. The most common types are smectic A, where the director is perpendicular to the layers, and smectic C, where the director makes some angle with the layers. In

general, there is long-range order of the tilt directions within a layer and/or across the layers. Therefore, the smectic C phase is optically biaxial.

Smectic B phase may be formed upon cooling from a C phase and regain the orthogonal alignment of the molecules with respect to the layer planes. There are two types of B phases. The hexatic B phase shows bond orientation order within the layers. When the centers of mass are separated by a multiple of the lattice vector, then the crystal smectic B phase (pseudo−hexagonal packing) or smectic E phase (Herringbone packing) is produced. However, the phase formed upon cooling from a smectic C phase may be tilted. This corresponds to the G and H phases depending on whether the lateral ordering within the layers has hexagonal and herringbone packings, respectively. The G phase is refered to as a tilted B phase. There are smectic F and I phases, which are the tilted analogs of the hexatic B.

In summary, A and C phases are two−dimensional fluids; B, E, F, G, H and I phases are two−dimensional solids. Smectic A, B and E are orthogonal phases and show uniaxial properties; Smectic C, F, G, H and I phases are tilted phases and show biaxial properties. (See table 1)

A substance may exhibit more then one liquid crystalline phase. It is not uncommon that upon cooling a nematic, one or more smectic phases are obtained before solidification. In the liquid crystal $4-n-$pentyloxybenzylidene$-4'-$heptylaniline (5O.7), the following phases are found upon cooling from isotropic liquid to solid ($N \rightarrow S_A \rightarrow S_C \rightarrow S_B \rightarrow S_G$) [1]. Because of its rich polymorphism, we have chosen this substance as the subject of this thesis. Deuteron NMR is chosen

to study molecular dynamics in various mesomorphic phases of 5O.7.

Table 1. Characteristics of the various smectic phases (after Ref. [9])

Structure within	Orthogonal	Tilted*	
the layers		$a > b$	$a < b$
Liquid	A		C
Bond-orientional order	hexatic B	F	I
(Pseudo)−hexagonal packing	B	G	G'
Herringnone packing	E	H	H'

*b is the unique axis of the monoclinic cell ($a \neq b \neq c$, $\alpha = \beta = \gamma = 90°$).

References

1. R.Y. Dong, "Nuclear Magnetic Resonance of Liquid Crystals", Springer–verlag, N.Y.,1994.

2. C.P. Slichter, "Principles of Magnetic Resonance", Third Edition, 1990.

3. A. Carrington and A.D. Mclanchlan, "Introduction to Magnetic Resonance", John Wiley and Sons, Inc., 1979; L.Friesen, "Nuclear Magnetic Resonance Techniques", thesis in Brandon University, 1992.

4. J.J. Sakurai, "Modern Quantum Mechanics", Addison-Wesley Publishing Company, Inc., 1985.

5. F.Reinitzer, Monatsh, 9, 421, 1888; O. Lehmann, Z. Phys. Chem. 4, 1889.

6. S. chandrasekhar, "Liquid Crystals", Cambridge University Press, 1976; L. Liebert, "Liquid Crystals", Academic Press, Inc., 1978; P.G. de Gennes, "Liquid Crystals", Oxford University Press, 1974.

7. Dachen Wu etc., "Polymer Liquid Crystals", 1988 (in Chinese).

8. R.Y. Dong, "Spectral Densities of Motion in Liquid Crystals by Deuterium NMR relaxation Study", Bulletin of Magnetic Resonance, Vol. 9, No. 1/2; G.M. Richards and R.Y. Dong, "Molecular Orientational Motion in Discotic Liquid Crystals", Liquid Crystals, 1989, Vol. 5, No. 3, 1011-1018.

9. G. Vertogen and W.H. de Jeu, "Thermotropic Liquid Crystals, Fundamentals", Spring–verlag, Heidelberg, 1988.

Chapter 2

Theory: Spin-lattice Relaxation for Spin−1 (Part I)

Free Motions in Uniaxial Phases

2.1 Introduction

The spin system needs a "spin−lattice interaction" to exchange energy with the lattice and in the case of deuteron, the dominant mechanism is the coupling of the electric field gradient with the electric quadrupole moment of the nucleus. The T_1 gives information on relatively fast molecular processes having correlation times approximately around 10^{-9}s. This is because T_1 relaxation involves an exchange of either one or two quanta of nuclear energy between the spins and the lattice. Thus T_1 involves the spectral density $J(\omega)$ of the fluctuating spin−lattice interactions in the vicinity of the Larmor frequency ω_0 and $2\omega_0$, where $\omega_0/2\pi$ may lie between ten and one hundred MHz depending on the strength of static magnetic field.

The NMR theory of spin-lattice relaxation of spin−1 nuclei via fluctuating quadrupolar interactions is considered within the Redfield approximation [1]. The full Hamiltonian $\mathcal{H}$ of a molecular system is usually complex. Fortunately, magnetic resonance experiments can be described by a much simplified spin Hamiltonian, which can be written in the principal coordinate axis system of the time−averaging electric field gradient tensor.

Molecular reorientation of liquid-crystal molecules has been considered [2,3,4]

by many authors. The small step rotational diffusion model proposed by Nordio *et al.* [2] has been widely used. It describes reorientation of a symmetric-top molecule in a potential of mean torque of Maier-Saupe type and employs a rotational diffusion tensor that is diagonal in a molecule-fixed frame. Strictly speaking, such a rotational diffusion tensor is only appropriate in isotropic liquids. Freed and co-workers [4] have accounted for the viscosity anisotropy of the mesophase by diagonalizing the rotational diffusion tensor of the symmetric-top in a laboratory (director) frame. The third-rate model extends the above model of Freed by superimposing fast rotations about the long molecular axis onto the reorientation of the symmetric-top in the director frame. This superimposed model is based on the assumption of statistical independence between these two motions. The assumption may be justified if there is a disparity in the time−scales of these motions. Both Nordio's model and the third-rate model have been used to discuss spin relaxation by molecular reorientation in liquid crystals, but a clear demonstration of which is more appropriate is still lacking [3,5,6]. At the end of this chapter, we discussed director fluctuations which may also contribute to the spectral densities of motion.

2.2 Motionally Averaged Hamiltonian

The averaging of Hamiltonian under rotations may be easily studied when it can be expressed in terms of irreducible tensor operator, $T^{\lambda}_{L,m}$ and $R^{\lambda}_{L,m}$ [7].

$$\mathcal{H}_{\lambda} = C_{\lambda} \sum_{L} \sum_{m=-L}^{L} (-1)^{m} R^{\lambda}_{L,-m} T^{\lambda}_{L,m} \tag{22}$$

where λ indicates the coupling mechanism (e.g. dipolar and quadrupolar) and C_{λ}

is an appropriate interaction constant. For quadrupolar interaction, $R^{\lambda}_{L,m}$ are non-zero only when $L = 2$ and will be replaced by V^2_m of eq. (20) in Chap. 1. In its PAS system, the components with $m = \pm 1$ vanish.

In the laboratory frame, the spin parts are constant while the spatial parts V^2_m are time−averaged under rotations to given $\langle V^2_m \rangle$. Now the Euler angles $\Omega = (\alpha', \beta', \gamma')$ are necessary to bring the laboratory system into the principal axis system. Using eqs. (18)-(21) in Chap. 1, the time−averaged quadrupolar Hamiltonian is

$$\overline{\mathcal{H}_Q} = \frac{eQ}{2I(2I-1)} \sum_{mm'} (-1)^m \langle D^{2*}_{-m,m'}(\alpha', \beta', \gamma') \rangle V^2_{m'} T_{2,m} \tag{23}$$

Note that here the inverse rotation transformation matrix $D^{L*}_{m,m'}$ is used and the $T_{2,m}$ are given by

$$\begin{aligned} T_{2,0} &= \frac{1}{\sqrt{6}}(3I_z^2 - I^2) \\ T_{2,\pm 2} &= \frac{1}{2}(I^{\pm})^2 \\ I^{\pm} &= I_x \pm i I_y \end{aligned} \tag{24}$$

2.3 Quadrupolar Splitting

For a deuteron ($I = 1$) spin with axially symmetric electric field gradient ($\eta = 0$), the time−averaged quadrupolar Hamiltonian is given by

$$\overline{\mathcal{H}_Q} = \frac{eQ}{2I(2I-1)} \langle V^2_0 \rangle T_{2,0} \tag{25}$$

In liquid crystals, molecules are aligned by their neighbors through the potential of mean torque. The preferred direction of the molecular alignment in a uniaxial phase is given by the director $\hat{n}$. For rodlike molecules whose $\Delta\chi > 0$, the director is parallel to the external magnetic field. The transformation should be carried out through an intermediate molecular frame (x_M, y_M, z_M)

$$\langle V_0^2 \rangle = \sum_m \overline{D^{2*}_{0,m}(\phi,\theta,\psi)} D^{2*}_{m,0}(\alpha,\beta,\gamma) V_0^2 \qquad (26)$$

where (α,β,γ) are the Euler angles that carry the molecular frame to PAS frame, while (ϕ,θ,ψ) the Euler angles that transform the laboratory frame into the molecular frame. Since γ and ϕ are irrelevant when $m' = 0$, the time−averaged quadrupolar Hamiltonian is given by

$$\begin{aligned} \overline{\mathcal{H}_Q} &= \hbar\omega_Q [I_z^2 - I(I+1)/3] \qquad (27) \\ \omega_Q &= \frac{3}{4}\frac{e^2qQ}{\hbar} \sum_m \overline{D^2_{0,m}(\theta,\psi)} D^2_{m,0}(\beta,\alpha) \end{aligned}$$

The time−averaged Wigner rotation matrices $\overline{D^2_{0,m}(\theta,\psi)}$ are the order parameters in a uniaxial phase and can be written in the form of a cartesian order tensor $\hat{S}$ which is a symmetric and traceless 3×3 matrix. Thus $\hat{S}$ has a maximum of five independent non−zero elements, defined by

$$\begin{aligned} S_{zz} &= \overline{D^2_{0,0}} \\ S_{xx} - S_{yy} &= \sqrt{\frac{3}{2}}(\overline{D^2_{0,2}} + \overline{D^2_{0,-2}}) \\ S_{xy} &= i\sqrt{\frac{3}{8}}(\overline{D^2_{0,-2}} - \overline{D^2_{0,2}}) \qquad (28) \\ S_{xz} &= \sqrt{\frac{3}{8}}(\overline{D^2_{0,-1}} - \overline{D^2_{0,1}}) \end{aligned}$$

$$S_{yz} = i\sqrt{\frac{3}{8}}(\overline{D^2_{0,-1}} - \overline{D^2_{0,1}})$$

The ordering of molecules in a mesophase may be described by a singlet probability function $P(\theta, \psi)$. The molecular frame may often be chosen such that $P(\theta, \psi)$ is an even function of the polar angles. This results in $\overline{D^2_{0,\pm 1}} = 0$ and $\overline{D^2_{0,2}} = \overline{D^2_{0,-2}}$. The Zeeman line is now split into two lines with a quadrupolar splitting

$$\delta\nu_Q = \frac{3}{2}\frac{e^2qQ}{\hbar}[S_{zz}(\frac{3}{2}\cos^2\beta - \frac{1}{2}) + \frac{1}{2}(S_{xx} - S_{yy})\sin^2\beta\cos 2\alpha] \qquad (29)$$

where (β, α) are polar angles of $C-D$ vector in the molecular frame. For molecules of cylindrical symmetry, the molecular biaxial parameter $(S_{xx} - S_{yy})$ is identical to zero.

2.4 Order Parameter

The orientation of molecules in a mesophase can be specified by a singlet distribution function $f(\Omega)$, where Ω denotes the Euler angles (ϕ, θ, ψ) that transform between the molecular and the director frame. The average of any single-molecule property $X(\Omega)$ over the orientations of all molecules is defined by

$$\langle X \rangle = \int_0^{2\pi} d\phi \int_0^{\pi} d\theta \sin\theta \int_0^{2\pi} d\psi X(\Omega) f(\Omega) \qquad (30)$$

In terms of the Wigner rotation matrices of rank L, the orientational distribution function can be expanded as

$$f(\Omega) = \sum_{L=0}^{\infty} \sum_{m,m'=-L}^{L} \frac{2L+1}{8\pi^2} a_{Lm'm} D^L_{m'm}(\Omega) \qquad (31)$$

Applying the normalization condition, the expanded coefficients $a_{Lm'm}$ can be obtained, i.e. $a_{Lm'm} = \langle D^L_{m'm}(\Omega)\rangle$. For rodlike molecules, the pseudo−potential $V(\Omega)$ is independent of ϕ and ψ due to the uniaxial phase symmetry and the cylindrical molecular symmetry, respectively. The orientation distribution function becomes

$$\begin{aligned} f(\Omega) &= \frac{f(\theta)}{4\pi^2} \\ f(\theta) &= \sum_{L=0}^{\infty} \frac{2L+1}{2} \langle P_L(\cos\theta)\rangle P_L(\cos\theta) \end{aligned} \tag{32}$$

where $P_L(\cos\theta) = D^L_{00}(\theta)$. Then the order parameters $\langle P_L\rangle$ are defined as

$$\langle P_L\rangle = \int_0^1 P_L(\cos\theta) f(\cos\theta) d(\cos\theta) \tag{33}$$

Among all the orientation parameters of different ranks, only $\langle P_2\rangle$ can be determined from the line positions in NMR spectra.

2.5 Spectral Densities

In the quadrupolar Hamiltonian, there are fluctuating terms because of the rotational and/or collective motions of liquid-crystal molecules. From the standard spin relaxation theory [8] for deuterons (I=1), the Zeeman (T_{1Z}^{-1}) and quadrupolar (T_{1Q}^{-1}) spin-lattice relaxation rates are given in terms of spectral densities $J_{m_L}(m_L\omega_0)$ by

$$\begin{aligned} T_{1Z}^{-1} &= J_1(\omega_0) + 4J_2(2\omega_0) \\ T_{1Q}^{-1} &= 3J_1(\omega_0) \end{aligned} \tag{34}$$

The spectral density is simply the Fourier transform of the autocorrelation function

$G_{m_L}(t)$

$$J_{m_L}(m_L\omega) = \frac{3\pi^2}{2}(q_{CD})^2 \int_0^\infty G_{m_L}(t)\cos(m_L\omega t)dt \tag{35}$$

where $q_{CD} = e^2qQ/h$ ($\eta = 0$ is assumed) is the nuclear quadrupolar coupling constant and $G_{m_L}(t)$ may be evaluated in terms of the Wigner rotation matrix $D^2_{m_Lm_M}(\Omega_{LM})$ in the fluctuating Hamiltonian

$$G_{m_L}(t) = \sum_{m_M}\left[d^2_{m_M0}(\theta)\right]^2 \Big\langle \left[D^2_{m_Lm_M}(\Omega_{LM}(0)) - \overline{D^2_{m_Lm_M}}\right] \times \left[D^{2*}_{m_Lm_M}(\Omega_{LM}(t)) - \overline{D^{2*}_{m_Lm_M}}\right]\Big\rangle \tag{36}$$

Now $\Omega_{LM}(\equiv \alpha, \beta, \gamma)$ denotes the Euler angles that transform between a molecular frame attached to the molecular core and the laboratory frame, θ is the angle between the C-D bond and the z_M axis of the molecular frame, and m_L and m_M are the projection indices for a tensor of rank two in the laboratory and molecular z axis, respectively. The autocorrelation functions for molecular reorientation (the term in the angle brackets in eq. (36)) are generally given by a sum of decreasing exponentials [2], and

$$G_{m_Lm_M}(t) = C_{m_Lm_M}\sum_{j=1}^{3} a^{(j)}_{m_Lm_M}\exp[-t/\tau^{(j)}_{m_Lm_M}] \tag{37}$$

where $C_{mn} = (\langle \mid D_{m,n} \mid^2\rangle - (\overline{D^2_{0,0}})^2)$, the mean square of the Wigner rotation matrices. The correlation times $\tau^{(j)}_{m_Lm_M}$ depend on the order parameter $\langle P_2\rangle$ and on the variations of the rotational diffusion tensor components with temperature. The correlations times are model dependent, as shown in the next paragraph. Equation (37) is expressed in the notation of Vold and Vold [3]. The $a^{(j)}_{m_Lm_M}$ represent

normalized weights of each exponential whose time constant

$$\tau^{(j)}_{m_L m_M} = b^{(j)}_{m_L m_M} \tau^2_{m_M} \tag{38}$$

with $\tau^2_{m_M}$ being the correlation times for rotational diffusion in liquid, i.e. with no ordering [9]. The $a^{(j)}_{m_L m_M}$, $b^{(j)}_{m_L m_M}$ and $C_{m_L m_M}$ coefficients for all the correlation functions are given numerically as polynomials in $\langle P_2 \rangle$ and their expansion coefficients are tabulated in Table I of Ref. [3] for a Maier-Saupe potential. The spectral densities are obtained by Fourier transforming $G_{m_L}(t)$ to give

$$J_{m_L}(m_L\omega) = \frac{3\pi^2}{2}(q_{CD})^2 \sum_{m_M}[d^2_{m_M,0}(\theta)]^2 C_{m_L m_M} \sum_j a^{(j)}_{m_L m_M} \frac{(\tau^{(j)}_{m_L m_M})^{-1}}{[(m_L\omega)^2 + (\tau^{(j)}_{m_L m_M})^{-2}]} \tag{39}$$

2.6 Diffusion Models

Nordio's Model

Nordio and co−workers solved the rotational diffusion equation (see Appendix B for details) for molecules under the influence of a potential of mean torque [2]. In this model, the diffusion tensor is diagonalized in a molecular frame. Its principal values $D_{\|}$ is the rotational diffusion constant of molecule about the z_M axis and $D_{\perp}$ is the rotational diffusion constant of the z_M axis. In the limit that the correlation functions are single exponential (retain $j = 1$ in eq. (37) only) with correlation times

$$(\tau_{m_L m_M})^{-1} = \frac{D_{\perp}}{\beta^2_{m_L m_M}} + m^2_M(D_{\|} - D_{\perp}) \,, \tag{40}$$

they found that the parameter $\beta^2_{m_L m_M}$ is related to the order parameter $\langle P_2 \rangle$. In the strong collision motion limit, $\beta^2_{m_L m_M} \rightarrow 1/6$ [10]. The above approximation is good except for very high $\langle P_2 \rangle$ and for $m_L = m_M = 1$ [11]. In the limit of perfect order, the correlation functions are given [12] by a single exponential with $C_{m_L m_M}$ and τ_{m_M} taking limiting values that can be expressed in terms of a small deviation δ from perfect alignment ($\delta = 1 - \langle P_2 \rangle$). Finally, the correlation times in eq. (38) for multi−exponential correlation functions can be used here:

$$(\tau^{(j)}_{m_L m_M})^{-1} = [6D_\perp + m_M^2(D_\parallel - D_\perp)]/b^{(j)}_{m_L m_M} \tag{41}$$

THIRD−RATE MODEL [3,4,6]

When the viscosity anisotropy of the mesophase is taken into account, the rotational diffusion tensor should assume [13] a diagonal form in the laboratory frame with its Z_L axis along the director. Now, D_α is used to represent diffusive precession of the long molecular axis about the director (α−motion). $D_\beta \equiv D_\perp$ refers to diffusive motion towards or away the director (β−motion). A modest extension of this model is to include rotational motion about a molecular z axis, with rotational diffusion constant D_γ. This is called the 'third−rate' anisotropic viscosity model. The γ−motion is usually rapid compared to the molecular precession about the director (α−motion) or the tumbling motion (β−motion). Thus the γ−motion can be assumed to be independent of either the α−motion or the β−motion [3]. As a result, the γ angle term in the Wigner rotation matrices can be separated out to

give

$$
\begin{aligned}
g_{m_L m_M m'_M}(t) &= \sum_{m_M m'_M} d^2_{m_M,0}(\theta) d^2_{m'_M,0}(\theta) \Gamma_{m_M m'_M}(t) \\
&\quad \times \Big\langle \exp\left[-i m_L \alpha(0)\right] d^2_{m_L,m_M}(\beta(0)) \\
&\quad \times \exp\left[i\, m_L \alpha(t)\right] d^2_{m_L,m'_M}(\beta(t)) \Big\rangle \qquad (42) \\
\Gamma_{m_M m'_M}(t) &= \langle \exp\left[-i m_M \gamma(0)\right] \exp\left[i m'_M \gamma(t)\right] \rangle
\end{aligned}
$$

where (α, β, γ) are Euler angles that transform between a molecular frame and the director frame. The $\gamma-$motion involves free rotation about a single axis with a diffusion constant D_γ, and

$$
\begin{aligned}
\Gamma_{m_M m'_M}(t) &= \delta_{m_M m'_M} \exp\left[-k_{m_M} t\right] \qquad (43) \\
k_0 &= 0 \quad (m_M = 0) \\
k_1 &= D_\gamma \quad (m_M = 1) \\
k_2 &= (3p+1) D_\gamma \quad (m_M = 2)
\end{aligned}
$$

with $p = 0$ corresponding to strong collision limit and $p = 1$ to small step diffusion motion. With this division of motions, the correlation functions can still be written as eq. (37), where the correlation times are now given by

$$
(\tau^{(j)}_{m_L m_M})^{-1} = k_{m_M} + \left[6 D_\beta + m_L^2 (D_\alpha - D_\beta)\right] / b^{(j)}_{m_L m_M} \qquad (44)
$$

Treatment of Ring Motions

The phenyl ring may have internal rotations about it para axis, which is described by a diffusion constant D_R. Ring−deuterated liquid crystal samples can

be used to detect this motion. For rod–like molecules like $nO.m$, the para axis is coincident with the molecular long axis or the angle between them is trivial. Internal ring rotations can hardly be detected in the presence of spinning motion of the molecule when liquid crystal samples are deuterated at the rings only. The internal ring motions can be treated using the superimposed rotations model [14,15]. For example, if the molecular motion is described by the third-rate model and the ring is assumed to rotate freely, the spectral densities of the ring deuterons are

$$J^{(R)}_{m_L}(m_L\omega) = \frac{3\pi^2}{2}(q_{CD})^2 \sum_{m_M}\sum_{m_R} C_{m_L m_M}\left[d^2_{m_R 0}(\theta_{R,Q})\right]^2\left[d^2_{m_M m_R}(\theta_{M,R})\right]^2 \times \sum_j a^{(j)}_{m_L m_M} \frac{(\tau^{(j)}_{m_L m_M m_R})^{-1}}{(m_L\omega)^2 + (\tau^{(j)}_{m_L m_M m_R})^{-2}} \tag{45}$$

$$(\tau^{(j)}_{m_L m_M m_R})^{-1} = (\tau^{(j)}_{m_L m_M})^{-1} + k_{m_R} \tag{46}$$

$$k_0 = 0 \quad (m_R = 0)$$

$$k_1 = D_R \quad (m_R = 1)$$

$$k_2 = (3p_r + 1)D_R \quad (m_R = 2)$$

with $p_r = 0$ corresponds to the strong collision limit and $p_r = 1$ the small step diffusive motion. $\theta_{R,Q}$, the angle between $C-D$ bond and the para axis, is taken as 60°. The $\theta_{M,R}$ is the angle between the para axis and the long molecular (z_M) axis. The z_M axis lies close to the para axis, making $\theta_{M,R} \simeq 0$ and $d^2_{m_M m_R}(\theta_{M,R}) = \delta_{m_M m_R}$.

Director Fluctuations

There are several motional processes (e.g. reorientation, director fluctuations) that take place simultaneously and may cause spin relaxation in liquid crystals.

Because of thermal fluctuations of the director, the orientation of director has both spatial and temporal variation. Since there is no long range order of positions among the molecules in nematics, a local (instantaneous) director $\hat{n}(\vec{r})$ may be introduced to represent the average direction of molecules within a neighborhood of any point in the sample. The time interval between molecular collisions is about $10^{-10} \sim 10^{-12}$s. Changes in molecular orientation due to collisions could change the local director on the NMR timescale. Thus, an additional coordinate system is needed to specify the local director $\hat{n}(\vec{r})$. The average director $\hat{n}_0$ is obtained by spatially averaging the local directors over the sample.

The angle $\Omega_{LM}(t)$ in the autocorrelation function (eq. (36)) denotes the orientation of the principal molecular axes (x_M, y_M, z_M) in the laboratory (X_L, Y_L, Z_L) frame. The coordinate transformation from the (x_M, y_M, z_M) to the (X_L, Y_L, Z_L) frame must be carried out through successive transformations [Fig. (4)] to account for the fast motions of a molecule and slow collective fluctuations of the director. That is, $\Omega_{LM} \equiv (\Omega', \Omega'')$, where the Euler angles Ω' transform from the molecular frame (x_M, y_M, z_M) to the instantaneous director (x, y, z) frame, Ω'' is used to transform the (x, y, z) frame to the laboratory frame (X_L, Y_L, Z_L). Here we assume the average director $\hat{n}_0$ is parallel to the external field $\vec{B}$, which is used to define the laboratory frame.

In the nematic phase and perhaps "disordered" smectic phases, molecules perform long range cooperative motions, which are slow compared to the rapid reorientational motions of individual molecules. The dynamics of these fluctuations depend

on the viscosity coefficients and the elastic constants of the liquid crystal. In the continuum theory, the elastic constants K_1, K_2 and K_3 are respectively the splay, twist and bend elastic constants [7,16]. Freed have included these collective effects in the spin relaxation theory by allowing the orienting potential $U(\Omega)$ to fluctuate slowly in time. It is assumed that the director shows small fluctuations about its mean position, and that the magnitude of ordering does not change. Then there are three types of terms that contribute to spectral densities: molecular reorientation, director fluctuations and a cross-term arising from both of these motions. According to Pincus [17], when director fluctuations are assumed to give small angular amplitude, director fluctuations only contribute to $J_1(\omega)$ in first order approximations. Furthermore, if director fluctuations are slow in comparison to the molecular reorientation, the coupling of these two types of motion would produce a very small cross term [18,19]. In the 'one-constant' approximation, *i.e.* $K_1 = K_2 = K_3 = K$ and one effective viscosity coefficient is used instead of five Leslie coefficients, the contribution to $J_1(\omega)$ from director fluctuations is [18]

$$J_{1DF}(\omega) = a_{DF}\left[P_2(\cos\theta)\right]^2\left[U(\omega_c/\omega)\omega^{-1/2} - \frac{\sqrt{8}}{\pi}\frac{\omega_c^{1/2}}{D_i}\right] \tag{47}$$

where the second term is a negative cross term, D_i is equal to D_β or $D_\perp$ depending on the models of molecular reorientation, θ is $\theta_{R,Q}$ or $\theta_{M,Q}$ depending on the ring deuteron or methine deuteron. The prefactor a_{DF} is

$$a_{DF} = \frac{3\pi^2}{2}(q_{CD})^2\frac{3kT < P_2 >^2}{4\sqrt{2}\pi K(D_t + K/\eta)^{1/2}} \tag{48}$$

where D_t is the averaged translational self-diffusion constant, ω_c is a high-frequency

cutoff frequency, and $U(\omega_c/\omega)$ is the cutoff function [20]. $U(\omega_c/\omega)$ is unity at low frequency and becomes small for Larmor frequency much larger than ω_c. The cutoff function is taken as one here and $\omega_c/2\pi = 200$ MHz may be used for the highest frequency director modes. Usually the angular factor $[P_2(\cos\theta)]^2$ is included in the prefactor. Here we write it explicitly in eq. (47) because the θ angle may be different for various deuterons in the molecule. Director fluctuations are important for spin relaxation in the kilohertz region. They are detected by spin relaxation in nematic and smectic A or smectic C phases. These collective modes are basically quenched in "ordered" (low symmetry) smectic phases.

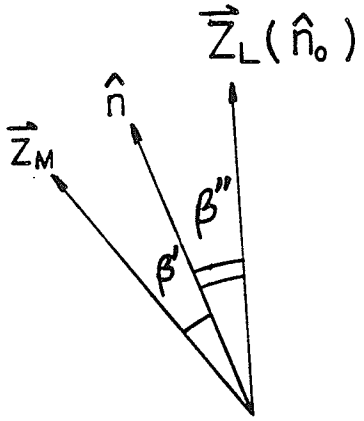

Figure 4 A schematic illustration of the coordinate systems used to account for director fluctuations in liquid crystals.

References

1. A.G. Redfield, IBM J. Res. Dev. 1, 19, (1957)

2. P.L. Nordio and P. Busolin, J. Chem. Phys. 55, 5485 (1971); P.L. Nordio, G. Rigatti and U. Segre, J. Chem. Phys. 56, 2117 (1972); Mol. Phys. 25, 129 (1973).

3. R.R. Vold and R.L. Vold, J. Chem. Phys. 88, 1443 (1988).

4. C.F. Polnaszek, G.V. Bruno and J.H. Freed, J. Chem. Phys. 58, 3185 (1973); C.F. Polnaszek and J.H. Freed, J. Phys. Chem. 79, 2283 (1975).

5. R.Y. Dong, J.W. Emsley and K. Hamilton, Liq. Cryst. 5, 1019 (1989).

6. G.L. Hoatson, T.Y. Tse and R.L. Vold, J. Magn. Reson. 98, 342 (1992); J.M. Goetz, G.L. Hoatson and R.L. Vold, J. Chem. Phys. 97, 1306 (1992).

7. R.Y. Dong, "Nuclear Magnetic Resonance of Liquid Crystals", Spring–Verlag, N.Y., 1994

8. J.P. Jacobsen, H.K. Bildsoe, and K. Schumburg, J. Magn. Reson. 23, 153 (1976); S.B. Ahmad, K.J. Packer and J. M. Ramsden, Mol. Phys. 33, 857 (1977); R.R. Vold and R.L. Vold, J. Chem. Phys. 66, 4018 (1977).

9. D.E. woessner, J. Chem. Phys. 1, 36 (1962); W.T. Huntress, Jr., Adv. Magn. Reson. 1, 4 (1970).

10. G. Agostini, P.L. Nordio, G. Rigatti, and U. Segre, Atti. Accad. Naz. Lincei Sez. 2a, 1, 13 (1975).

11. P.L. Nordio, The Molecular Physics of Liquid Crystals, edited by G.R. Luckhurst and G.W. Gray (Academic Press, London, 1979), Chap. 18.

12. P.L. Nordio and U. Segre, J. Magn. Reson. 27, 465 (1977).

13. A.N. Kutzentzov, J. Struct. Chem. 11, 488 (1970).

14. R.Y. Dong, Mol. Cryst. Liq. Cryst. 141, 349 (1986).

15. P.A. Beckmann, J.W. Emsley, G.R. Luckhurst, and D.L. Turner, Mol. Phys. 59, 97 (1986).

16. P.G. de Gennes, "The Physics of Liquid Crystals", Oxford University Press, 1974.

17. P. Pincus, Solid State Commun. 7, 415, 1969.

18. J.H. Freed, J. Chem. Phys. 16, 4183 (1977).

19. P. Ukleja, J. Pirs and J.W. Doane, Phys. Rev. A 14, 414 (1976).

20. J.W. Doane, C.E. Tarr and M.A. Nickerson, Phys. Rev. Lett. 33, 620 (1974).

Chapter 3

Theory: Spin-lattice Relaxation for Spin−1 (Part II)

Restricted Uniaxial Motions and Biaxial Phases

3.1 Introduction

Among the phases which have been classified as "smectics", it is believed [1] the "disordered" phases such as smectic A and C phases have a liquid−like order. The "ordered" smectic phases such as E, G, H, and crystal B phases are "crystalline" in the sense that they exhibit long−range three−dimensional position order. Molecular reorientation has a dominant contribution to the spectral densities in "ordered" smectic phases. Two questions arise: Firstly, do molecules still rotate freely or are their motions biased due to the close packing; and secondly, are biaxial properties of certain smectic phases "wiped out" when the director is coincident with the Z_L axis of the laboratory frame. The restricted libration within $\gamma = \pm\phi_0/2$ (Fig. 5) for internal motions in macromolecules has been considered by London and Avitabile [2], and Wittebort and Szabo [3]. Morrison and Bloom has considered orientation−dependent spin−lattice relaxation rates for spin−1 nuclei [5,6], while Berggren *et al.* [4] have calculated all non−vanishing spectral densities in biaxial liquid crystal phases of D_{2h} summetry. Some of these spectral densities vanish at the biaxial−uniaxial phase transition. It is recognized [7] that the "biaxial" spectral densities are not observed in biaxial phases unless the director is oriented

away from the external magnetic field.

3.2 Restricted Uniaxial Rotation

Both Nordio's model and the third−rate model may be used to account for free rotational diffusion motion of molecules. So far, studies of some liquid crystals in their low symmetry smectic phases by NMR and other experimental techniques have revealed that molecules may rotate around their long axes in a strongly biased manner [8,9]. Here we use the third−rate model in which the γ−motion is restricted to give librations of finite amplitudes. The probability $p(\phi' t|\phi 0)$ is the probability density that the γ angle is ϕ' at time t given that at $t = 0$ it had a value of ϕ. By solving a one-dimensional diffusion equation subject to the reflecting boundary conditions at $\gamma = \pm\phi_0/2$, i.e. $[\partial p(\phi,t)/\partial\phi]_{\phi=\pm\phi_0/2} = 0$. It has been shown that [2,3]

$$\begin{aligned} p(\phi' t|\phi 0) &= \frac{1}{\phi_0} + \frac{1}{\phi_0}\sum_{n=1}^{\infty} \cos\left[\frac{n\pi(\phi - \phi_0/2)}{\phi_0}\right] \cos\left[\frac{n\pi(\phi' - \phi_0/2)}{\phi_0}\right] \\ &\quad \times \exp\left[-\frac{D_\phi n^2\pi^2}{\phi_0^2}\, t\right] \end{aligned} \tag{49}$$

where D_ϕ is a diffusion constant (similar to D_γ) to describe restricted uniaxial rotational diffusion. As $t \to \infty$, $p(\phi' t|\phi 0) \longrightarrow p_{eq}(\phi) = 1/\phi_0$. The required Γ function which is analogous to that of in eq. (42) in chapter 2 is

$$\begin{aligned} \Gamma_{m_M m'_M}(t) &= \int_{-\phi_0/2}^{\phi_0/2}\int_{-\phi_0/2}^{\phi_0/2} d\phi d\phi' \exp\left[-i\, m_M \phi(0)\right] \exp\left[i\, m'_M \phi(t)\right] \\ &\quad \times p_{eq}(\phi) p(\phi' t|\phi 0) \\ &= \sum_{n=0}^{\infty} \tilde{\Gamma}_{m_M m'_M n}(\phi_0) \exp\left[-\frac{n^2\pi^2 D_\phi}{\phi_0^2} t\right] \end{aligned} \tag{50}$$

$$\tilde{\Gamma}_{m_M m'_M 0}(\phi_0) = \frac{4\sin(m_M\phi_0/2)\sin(m'_M\phi_0/2)}{m_M m'_M \phi_0^2}$$

$$\tilde{\Gamma}_{m_M m'_M n}(\phi_0) = 4\phi_0^2 m_M m'_M \times$$

$$\left\{ \frac{(1-(-1)^n)(\cos m_M\phi_0/2)(\cos m'_M\phi_0/2)}{[(m_M\phi_0)^2-(n\pi)^2][(m'_M\phi_0)^2-(n\pi)^2]} \right.$$

$$\left. + \frac{(1+(-1)^n)(\sin m_M\phi_0/2)(\sin m'_M\phi_0/2)}{[(m_M\phi_0)^2-(n\pi)^2][(m'_M\phi_0)^2-(n\pi)^2]} \right\} \quad n \geq 1$$

The series expansion converges rapidly, generally only the first five terms are required. Using the local uniaxial symmetry $\delta_{m_M m'_M}$, $\tilde{\Gamma}_{m_M m_M n}(\phi_0)$ may be simplified and $\Gamma_{m_M m_M}(t)$ is given by

$$\Gamma_{m_M m_M}(t) = \frac{2}{\phi_0^2}\left\{ \frac{1-\cos m_M\phi_0}{m_M^2} + 2\sum_{n=1}^{\infty} \frac{m_M^2\left[1-(-1)^n\cos m_M\phi_0\right]}{\left[\frac{n^2\pi^2}{\phi_0^2}-m_M^2\right]^2} \right\}$$

$$\times \exp\left[-\frac{n^2\pi^2 D_\phi}{\phi_0^2}t\right] \tag{51}$$

Using the anisotropic viscosity model to describe the $\alpha-$motion and $\beta-$motion, the correlation functions are given by

$$G_{m_L}(t) = \sum_{m_M}\left[d^2_{m_M,0}(\theta)\right]^2 C_{m_L m_M}\sum_{j=1}^{3} a^{(j)}_{m_L m_M}\Gamma_{m_M m_M}(t)\exp\left[-t/\tau^{(j)}_{m_L m_M}\right] \tag{52}$$

where $\Gamma_{m_M m_M}(t)$ is given by eq. (51). The corresponding spectral densities of motion are now given by

$$J_{m_L}(m_L\omega) = \sum_{m_M}\left[d^2_{m_M,0}(\theta)\right]^2 C_{m_L m_M}\sum_{j=1}^{3} a^{(j)}_{m_L m_M}\left\{ \frac{2(1-\cos m_M\phi_0)}{(m_M\phi_0)^2} \right.$$

$$\left. \times \frac{(\tau^{(j)}_{m_L m_M})^{-1}}{(m_L\omega)^2+(\tau^{(j)}_{m_L m_M})^{-2}} \right.$$

$$+\frac{4}{\phi_0^2}\sum_{n=1}^{\infty}\frac{m_M^2\left[1-(-1)^n\cos m_M\phi_0\right]}{\left[\left(\frac{n\pi}{\phi_0}\right)^2-m_M^2\right]^2}$$

$$\times \frac{(\tau^{(j)}_{m_L m_M n})^{-1}}{(m_L\omega)^2 + (\tau^{(j)}_{m_L m_M n})^{-2}} \Bigg\} \tag{53}$$

with

$$\begin{aligned} \left(\tau^{(j)}_{m_L m_M n}\right)^{-1} &= \left(\tau^{(j)}_{m_L m_M}\right)^{-1} + \left(\frac{n\pi}{\phi_0}\right)^2 D_\phi \\ &= \frac{6D_\beta + m_L^2(D_\alpha - D_\beta)}{b^{(j)}_{m_L m_M}} + \left(\frac{n\pi}{\phi_0}\right)^2 D_\phi \end{aligned} \tag{54}$$

3.3 Relaxation in Biaxial Liquid Crystal Phases

In biaxial liquid crystal phases, the correlation functions depend on two projection indices m_L and m'_L in the laboratory frame. Writing the laboratory correlation functions in terms of their counterparts in a suitable molecular frame whose orientation with respect to the laboratory frame is given by the Euler angles $\Omega \equiv (\alpha, \beta, \gamma)$, one has

$$\begin{aligned} G_{m_L m'_L}(t) &= \sum_{m_M m'_M} \left[d^2_{m_M 0}(\theta)\right] \left[d^2_{m'_M 0}(\theta)\right] \Big\langle \left[D^2_{m_L m_M}(\Omega(0)) - \overline{D^2_{m_L m_M}}\right] \\ &\quad \times \left[D^{2*}_{m'_L m'_M}(\Omega(t)) - \overline{D^{2*}_{m'_L m'_M}}\right] \Big\rangle \\ &= \sum_{m_M m'_M} \left[d^2_{m_M 0}(\theta)\right] \left[d^2_{m'_M 0}(\theta)\right] G_{m_L m'_L m_M m'_M}(t) \end{aligned} \tag{55}$$

where the angle θ is between the C−D bond and the molecular z_M−axis. In a uniaxial phase, a rotation about the director should leave the system invariant. If the molecule has an effective cylindrical symmetry, a rotation around the z_M axis should also leave the system invariant. Thus the nonvanishing correlation functions

$G_{m_L m'_L m_M m'_M}(t)$ become $G_{m_L m_M}(t)$ (see eq. (37)) due to the $\delta_{m_L m'_L}\delta_{m_M m'_M}$. In biaxial phases, one has the possibility of observing correlation functions with $m_L \neq m'_L$. For liquid crystals of the D_{2h} phase symmetry of molecules with cylindrical symmetry, the correlation functions $G_{m_L m'_L m_M}$ are non−zero. Furthermore, the standard properties of Wigner rotation matrices [10] give

$$G_{m_L m'_L m_M}(t) = (-1)^{-m_L - m'_L} G_{m_L m'_L - m_M} \tag{56}$$

which indicates that the correlation functions $G_{m_L m'_L}$ vanish as long as the sum of m_L and m'_L is an odd number. The corresponding spectral densities can be derived by taking Fourier transformations to give

$$J_{m_L m'_L}(\omega) \;=\; \frac{3\pi^2}{2}\,(q_{CD})^2 \sum_{m_M} \left[d^2_{m_M 0}(\theta) \right]^2 \int_0^\infty G_{m_L m'_L m_M}(t) \exp\left[-i\omega t\right] dt \tag{57}$$

The potential of mean torque $U(\Omega)$, acting on uniaxial molecules in the biaxial phase, is independent of the γ angle, *i.e.* $U(\Omega) = U(\alpha, \beta)$. Using Nordio's model, Berggren *et al.* [4] have solved the rotational diffusion equation with the $U(\alpha, \beta)$ to get the expressions for spectral densities due to molecular reorientation. (see Appendix B)

The general theory of spin−lattice relaxation for spin−1 nuclei gives (analogous to eq. (34) in chapter 2).

$$\begin{aligned} [T_{1Q}(\Omega)]^{-1} &= 3J_1(\omega_0, \Omega) \\ [T_{1Z}(\Omega)]^{-1} &= J_1(\omega_0, \Omega) + 4J_2(2\omega_0, \Omega) \end{aligned} \tag{58}$$

where $\Omega \equiv (\beta, \alpha)$ denotes the polar angles of the director in the laboratory frame whose Z_L−axis is along the magnetic field. Note that $J_m(m\omega_0, 0°) = J_m(m\omega_0)$ when

the director is aligned along to the magnetic field ($\beta = 0°$). In order to interpret the observed spin−lattice rates in the above equations, explicit expressions for $J_m(m\omega_0, \Omega)$ in terms of $J_{m_L m'_L}(m\omega_0)$ are necessary. A motional model such as that of Berggren *et al.* must also be chosen. Now $J_m(m\omega_0, \Omega)$ expressions are given by eq. (11) of ref. [5] in terms of order parameters, Clebsch-Gordan coefficients and reduced spectral densities $J_{m_L m'_L}(m\omega_0)$. By adoping a D_{2h} symmetry for biaxial mesophases, the spectral densitries $J_{1,0}(m\omega)$, $J_{1,2}(m\omega)$ and $J_{2,-1}(m\omega)$ are identical to zero. We have rewritten these expressions [7] to give

$$\begin{aligned} J_1(\omega,\Omega) &= \frac{3}{2}\cos^2\beta\sin^2\beta J_{0,0}(\omega) + \frac{1}{2}(1-3\cos^2\beta+4\cos^4\beta)J_{1,1}(\omega) \\ &+\frac{1}{2}(1-\cos^4\beta)J_{2,2}(\omega) + \cos 2\alpha\cos^2\beta\sin^2\beta J_{2,0}(\omega) \\ &-\frac{1}{28}\cos 2\alpha\left[1-29\cos^2\beta+28\cos^4\beta\right]J_{1,-1}(\omega) \\ &-\frac{1}{2}\cos 4\alpha\left[1-\cos^2\beta\right]^2 J_{2,-2}(\omega) \end{aligned} \tag{59}$$

$$\begin{aligned} J_2(2\omega,\Omega) &= \frac{3}{8}(1-\cos^2\beta)^2 J_{0,0}(2\omega) + \frac{1}{2}(1-\cos^4\beta)J_{1,1}(2\omega) \\ &+\frac{1}{8}(1+6\cos^2\beta+\cos^4\beta)J_{2,2}(2\omega) \\ &+\frac{1}{4}\cos 2\alpha\left[1-\cos^4\beta\right]J_{2,0}(2\omega) \\ &+\frac{1}{28}\cos 2\alpha\left[5+2\cos^2\beta-7\cos^4\beta\right]J_{1,-1}(2\omega) \\ &+\frac{1}{8}\cos 4\alpha\left[1-\cos^2\beta\right]^2 J_{2,-2}(2\omega) \end{aligned} \tag{60}$$

These two equations reduce to the familiar expressions for uniaxial phases [11]. The reason is that "biaxial" spectral densities $J_{2,0}(m\omega)$, $J_{1,-1}(m\omega)$ and $J_{2,-2}(m\omega)$ are nonzero only in biaxial phases. In particular, these spectral densities involve param-

eters that depend on the biaxial order parameters $\langle D^4_{2,0}\rangle$, $\langle D^2_{2,0}\rangle$ and/or $\langle D^4_{4,0}\rangle$ (see table II, ref. [4]). It is obvious from eqs. (59) and (60) that in biaxial mesophases when the director is aligned along the external field ($\beta = 0°$), the spin−lattice relaxation rates are insensitive to the "biaxial" spectral densities. Thus in this case, a biaxial phase behaves like a uniaxial phase as far as spin−lattice relaxation is concerned. Moreover, for rod−like molecule reorienting in a potential of mean torque, all the "uniaxial" terms, which make contributions to the spectral densities, change continuously and smoothly through the uniaxial−biaxial phase transition [4]. Thus the spectral densities should change the same way through the phase transition as long as $\beta = 0°$.

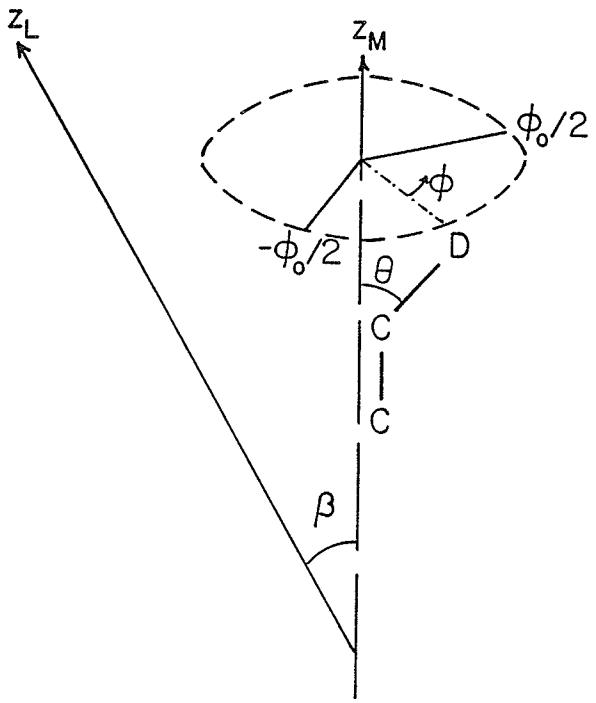

Figure 5 Restricted rotation of $\pm\phi_0/2$ about the molecular z_M axis.

References

1. G.W. Gray, "The Molecular Physics of Liquid Crystals" (G.R. luckhurst and G.W. Gray, Eds.), pp.263-283, Academic Press, London/New York 1979.

2. R.E. London and J. Avitabile, J. Am. Chem. Soc. 100, 7159 (1978).

3. R.J. Wittebort and A. Szabo, J. Chem. Phys. 69, 1722 (1978).

4. Berggren, E., Tarroni, R., and Zannoni, C., 1993, J. Chem. Phys. 99, 6180.

5. Morrison, C., and Bloom, M., 1993, J. Magn. Reson. A 103, 1.

6. Morrison, C., 1993, Ph.D. Thesis (U.B.C.).

7. R.Y. Dong, "Nuclear Spin Relaxation in Biaxial Liquid Crystal Phases", (in press).

8. R. Blinc, J. Dolinsek, M. Luzar, and J. Selinger, "Liquid Crystals", 3, 663 (1988).

9. G. Cvikl, U. Dahlborg, M. Cepic, J. Peternelj, I. Jencic, B. Glumac, and M. Davidovic, Physics Scripta 44, 63 (1991).

10. C. Zannoni, in "The Molecular Physics of Liquid Crystals" (G.R. luckhurst and G.W. Gray, Eds.), p.51, Academic Press, London/New York 1979.

11. Freed, J.H., 1977, J. Chem. Phys. 66, 4183; Luckhurst, G.R., and Sanson, A., 1972, Mol. Phys. 24, 1297; Barbara, T.M., Vold, R.R., and Vold, R.L., 1983, J. Chem. Phys. 79, 6338.

Chapter 4

Experimental Methods

4.1 Apparatus

A home-built superheterodyne coherent pulse NMR spectrometer was operated at 15.3 MHz using a Varian 15 in electromagnet and at 46.05 MHz using a 7.1 Tesla Oxford superconducting magnet. The sample was placed in a NMR probe whose temperature was regulated in the superconducting magnet by air flow with a Bruker BST-1000 temperature controller while in the electromagnet by an external oil bath circulator. The temperature gradient across the sample was estimated to be better than 0.3°C. The pulse programming was controlled by a 1280 mini-computer. The $\pi/2$ pulse widths *ca.* 3.4 μs at 46 MHz and 4.6 μs at 15.3 MHz were produced by an Amplifier Research Model 200L power amplifier. Pulse control, signal collection, Fourier transformation and data processing [1] were done by a General Electric 1280 computer.

4.2 Quadrature Detection and Phase Cycling

Typically a particular NMR experiment is repeated many times to improve the single-to-noise S/N ratio and the output signals are summed and then Fourier-transformed to give NMR spectra. In order to produce accurate and reproducible data, care is needed to minimize imperfections inherent in the NMR spectrometer.

To maximize the free-induction decay (FID) signal, the excitation pulse must have a frequency profile (centered at the Larmor frequency ν_0) that covers the NMR lines of interest at frequency ν. Since only one channel is used in the single phase detection, the detector "sees" only one magnetization component in the rotating frame and it is unable to "tell" if the magnetization is precessing faster ($\Delta\nu = \nu - \nu_0 > 0$) or slower ($\Delta\nu < 0$) than the excitation frequency. The Fourier transformation of this FID signal produces two lines on either side of the excitation frequency, one of which is a real line and the other is a fictitious line. To avoid this kind of spectrum folding, or aliasing, the quadrature detection method has been introduced [2,3]. Using this technique, the FID signal from the sample is detected by two channels in a receiver which are parallel but differ in phase by 90°. The signals in the two channels form a complex signal with certain amplitude and phase. This phase carries information that distinguishes signals having a positive offset from a negative offset. That is nuclei that resonate at frequency with $\Delta\nu > 0$ provide a different signal than nuclei that resonate at the frequency with $\Delta\nu < 0$. Thus Fourier transforming this complex signal produces spectrum which does not have the unwanted line and has the real line double in intensity. The S/N ratio is improved by a factor of $\sqrt{2}$ [4,5].

The quadrature signals from the receiver are sent to two channels in the 1280 computer for signal averaging. Now the phase difference of the two channels in a receiver may deviate from the desired value of 90° and the gains of these channels may not be exactly the same. These problems are solved by using phase cycling of both radiofrequency pulses and the receiver channels. The computer controls the

phase shifter to produce $r.f.$ phases at 0°, 90°, 180°, 270°. Each receiver channel takes turn in detecting the real and imaginary parts of the FID signal as the receiver phase is cycled between 0° and 90°. As a result, the two channels equally share any error in quadrature or amplification. Then the computer collects the real and imaginary parts of the FID signal and sums them in two separate memories (memory A for real signal and memory B for imaginary signal) [5]. Thus the imperfections in $r.f.$ phases and in the quadrature detector of the receiver are compensated.

4.3 Pulse Sequence

In order to observe relaxation effects, the spin system has to be disturbed from equilibrium. In NMR this is usually done by applying an oscillating magnetic field for a short period. As mentioned in the last section, this oscillating field carries a frequency at or near the Larmor frequency ω_0 of the spin. The setup of a typical longitudinal (T_1) relaxation experiment is shown in Fig. 6. The shaded rectangle represents one or more $r.f.$ pulses. Their pulse lengths and inter-pulse spacing determine the initial conditions of the spin system for the relaxation experiment. The spin system is left to relax during a time period t. A detection pulse (or pulses) is then applied to measure the spin magnetization along the Z_L axis by observing the time domain FID signal.

For deuterated liquid crystal molecules, the spin-lattice relaxation rates can be measured using the Jeener–Broekaert (J-B) pulse sequence with phase cycling as described by Vold *et al.* [2,3]. (see also Table 2. and Fig. 7(a)) Note that the above

pulse sequence has included an additional monitoring 45° pulse to minimize the long−term instability of the spectrometer. This pulse was phase−cycled to have a net effect of subtracting the equilibrium magnetization (M_0) signal from the J−B signal. After the spin system has been put in a non−equilibrium state by the first two pulses of the sequence, the relaxation to its equilibrium state is monitored by a detection pulse at various time t. Since each deuteron gives rise to a doublet due to incomplete averaging of the quadrupole coupling, (see eq. (29) in Chap. 2) the intensity of the two lines of this doublet, here named 'L' and 'H', depend on the time t as [2,6]

$$\begin{aligned} M_L &= A\exp(-t/T_{1Z}) - B\exp(-t/T_{1Q}) \\ M_H &= A\exp(-t/T_{1Z}) + B\exp(-t/T_{1Q}) \end{aligned} \tag{61}$$

where A and B are constants determined by the initial state of the system. By adding and subtracting M_L and M_H, respectively, the Zeeman and quadrupolar relaxation times, T_{1Z} and T_{1Q}, can be obtained.

In our experiments, we use the broadband Jeener−Broekaert sequence with the appropriate phase−cycling of radiofrequency and receiver phases [7] to simultaneously measure T_{1Z} and T_{1Q}. (see Table 3 and Fig. 7(b)) This avoids the necessity of matching the pulse separation between the first two pulses in the traditional J-B method to the quadrupolar splitting of the observed deuteron.

4.4 Experimental

Two samples of 5O.7 (Fig. 8) were used. The 5O.7-d_1 sample is labeled at

the methine site and has a nematic-isotropic transition temperature $T_c = 77.6°C$, while the 5O.7-d_4 sample is labeled at the aniline ring and has a $T_c = 76.2°C$. The transition temperatures of 5O.7-d_1 are close to the literature values [8] for 5O.7 ($S_G - S_B$ at 38°C, $S_B - S_C$ at 52°C, $S_c - S_A$ at 55°C, S_A-N at 64°C and N-I at 78°C). When comparing the data of 5O.7-d_1, and 5O.7-d_4, we scale the temperatures to give a common T_c of 77.6°C. In this study, we report measurements of the Zeeman and quadrupolar spin-lattice relaxation times T_{1Z} and T_{1Q} of the methine and ring deuterons at two different Larmor frequencies. In using the broadband J-B sequence, the time interval τ (Fig. 7(b)), which determines the pulse spacing among the first four pulses, was set to *ca.* 5 μs for quadrupolar splittings less than 70 kHz. This value was reduced for larger splitting [4]. For example, if the values of τ are set to 2 μs and 5.5 μs, the corresponding irradiation band-widths are 150 kHz and 70 kHz, respectively. Signal collection was started *ca.* 10 μs after each monitoring $\pi/4$ pulse. In the nematic and smectic A or C phases, each FID signal was averaged over 128-640 scans at 46 MHz and 1280-2048 scans at 15.3 MHz. The larger number of scans was required for 5O.7-d_1. This number of scans was increased to 1024-2048 at 46MHz and 4096-6144 at 15.3MHz due to the poorer S/N ratio in smectic B and G phases. The experimental uncertainty in the spin-lattice relaxation times was estimated to be ±5% or better. The quadrupolar splittings of the methine and ring deuterons (see Fig. 9) were determined from deuteron NMR spectra obtained by Fourier transforming the FID signal after a $\pi/2$ pulse. These splittings have an experimental error of better than ±1%. It should be mentioned

that the splittings are temperature dependent, which was used for temperature calibration. In our experiments, the copper-constantan thermocouple can be put only close to the sample, so its reading does not represent the real temperature of the sample. Fortunately there are some phase transition points in the liquid crystal (such as $I - N$, $N - S_A$, $S_C - S_B$), whose temperatures can be determined more accurately by observing changes in the sample texture under a microscopy. In NMR experiments, these phase transitions may be detected through discontinuity in the quadrupolar splittings. Then a calibration between the temperature and the splitting was obtained. In the S_B and S_G phases of 5O.7, this method is less reliable since the splitting here is relatively insensitive to the temperature. But it is still reasonable to assume that the thermocouple readings vary linearly with the real sample temperatures as long as the whole thermal circulation system was kept unchanged except the heater current. Hence several splittings were measured and the corresponding thermocouple readings were recorded within S_A, S_C phases and near the $S_C - S_B$ phase transition. Their relationship was then extrapolated to the S_B and S_G phases. From the thermocouple readings in these low symmetry smectic phases, the real sample temperatures were derived.

TABLE 2

J-B Sequence with Phase-cycling						
ϕ_1	ϕ_2	ϕ_3	Aqu T	ϕ_4	Aqu T	Receiver Phase(*)
x	y	x	+			0
-y	x	y	-			90
x	y	-x	-			0
-y	x	-y	+			90
				y	+	90
				x	-	0
				-y	-	90
				-x	+	0
				-x	+	0
				-y	-	90
				x	-	0
				y	+	90
x	-y	-y	+			90
-y	-x	-x	-			0
x	-y	y	-			90
-y	-x	x	+			0

TABLE 3

Broadband J-B Sequence with Phase-cycling								
ϕ_1	ϕ_2	ϕ_3	ϕ_4	ϕ_5	Aqu T	ϕ_6	Aqu T	receiver Phase(*)
x	-y	y	y	x	+			0
-y	-x	x	x	y	-			90
x	-y	y	y	-x	-			0
-y	-x	x	x	-y	+			90
						y	+	90
						x	-	0
						-y	-	90
						-x	+	0
						-x	+	0
						-y	-	90
						x	-	0
						y	+	90
x	y	-y	-y	-y	+			90
-y	x	-x	-x	-x	-			0
x	y	-y	-y	y	-			90
-y	x	-x	-x	x	+			0

(*) +/- during aquisition (Aqu) denotes addition to or subtraction of the signal from computer memory; cycling of the receiver phase minimized the quadrature images.

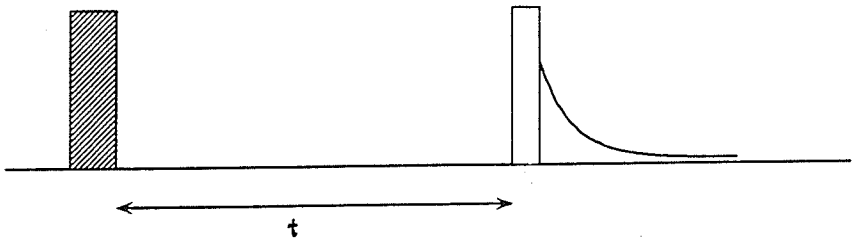

Figure 6 Typical setup of a (longitudinal) relaxation experiment. The shaded rectangle represents a series of *r.f.* pulses. Time t is a variable evolution time. The white rectangle represents the detection pulse(s).

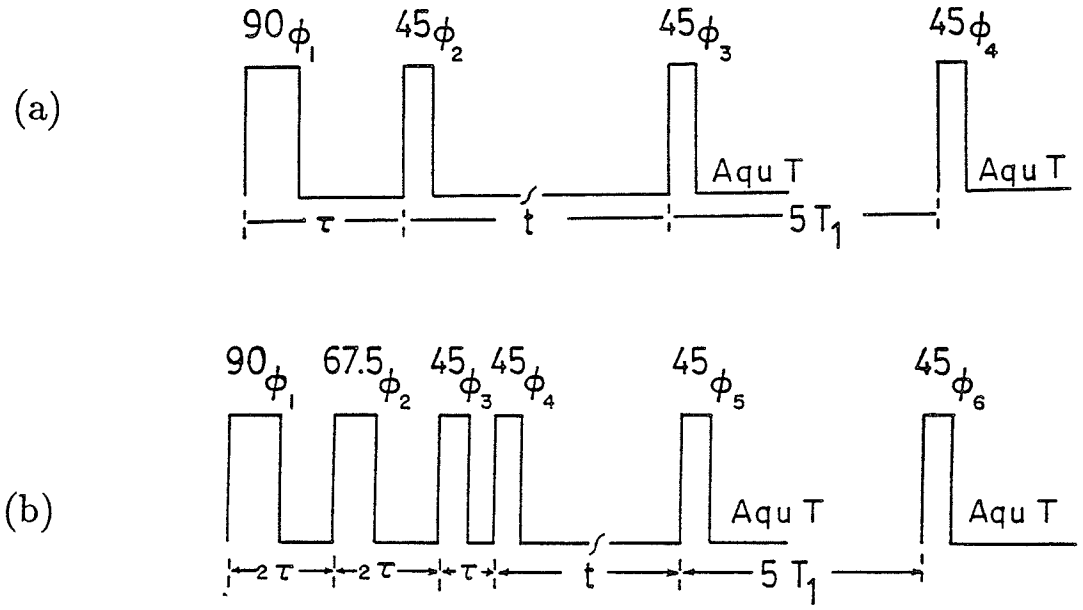

Figure 7 (a) J−B sequence, (b) broadband J−B excitation sequence.

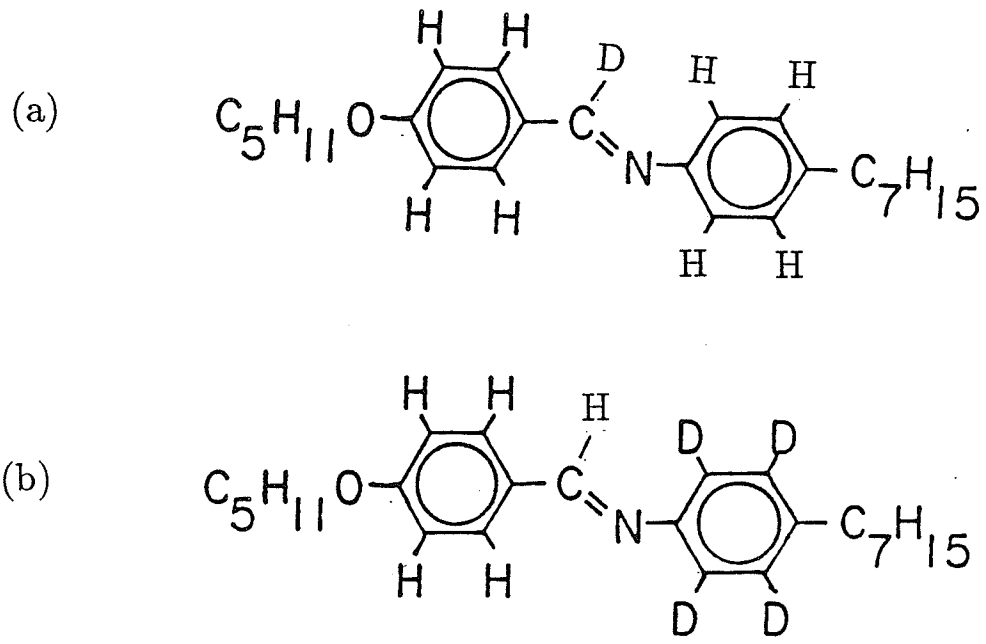

Figure 8 The molecular structure of (a) 5O.7−d_1 and (b) 5O.7−d_4.

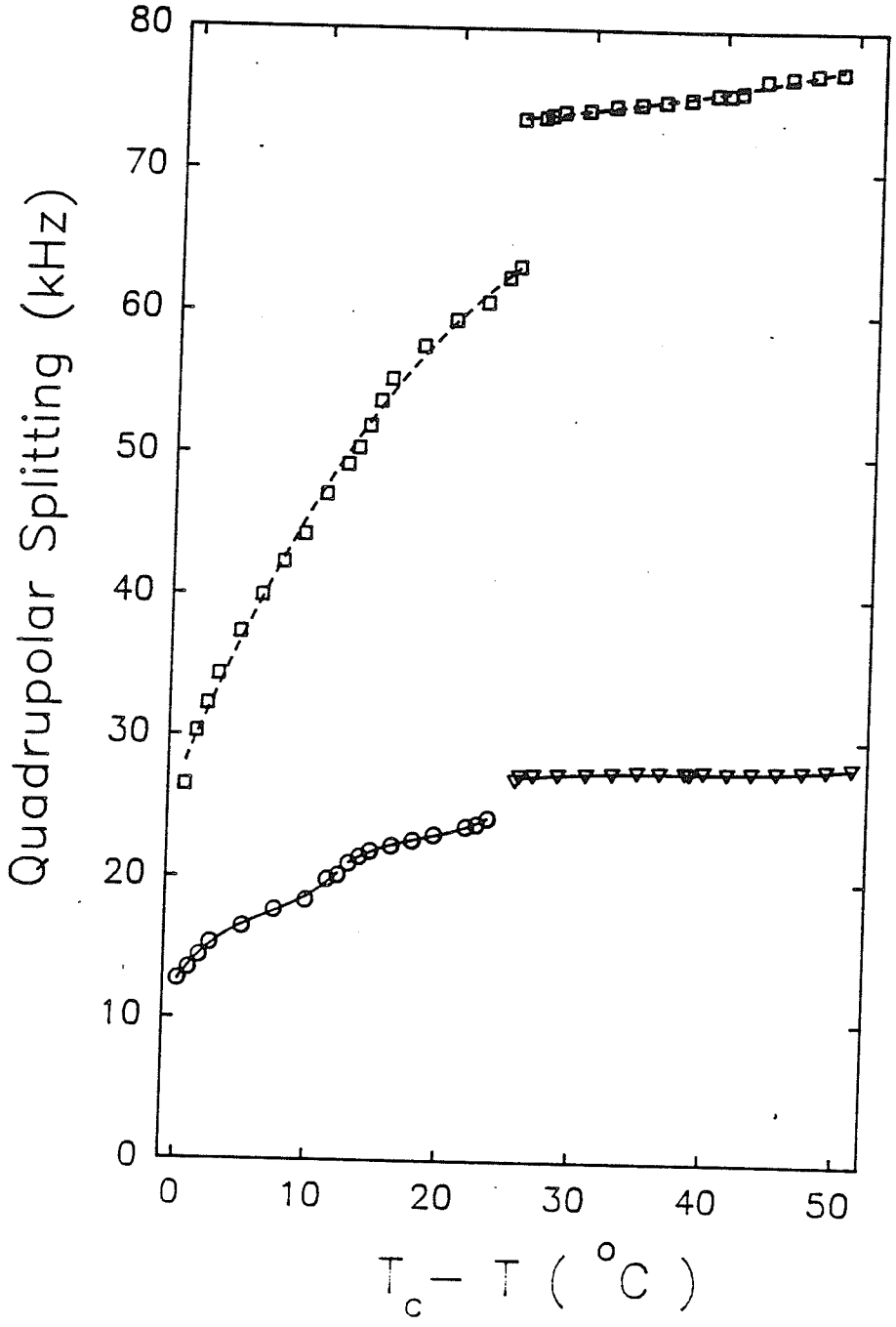

Figure 9 Plots of quadrupolar splittings versus $T_c - T$. ○ and ▽ denote splittings of 5O.7$-d_4$ in "disordered" liquid-like phases and "ordered" solid-like phases, respectively. □ denotes splittings of 5O.7$-d_1$.

References

1. R.Y. Dong and G.M. Richards, J. Chem. Soc. Faraday Trans. II 84, 1053 (1988).

2. R.L. Vold, W.H. Dickerson and R.R. Vold, J. Magn. Reson. 43, 213 (1981)

3. T.M. Barbara, R.L. Vold, and R.R. Vold, J. Magn. Reson. 59, 478 (1984).

4. E.O. Stejskal and J. Schaefer, J. Magn. Reson. 13, 249 (1974); ibid 14, 160 (1974)

5. Eiichi Fukushima and Stephen B.W. Roeder, Experimental Pulse NMR, Addison-Wesley Publishing Company, Inc. (1981); GN-Series Software Manual, General Electric (1991).

6. R.Y. Dong, Nuclear Magnetic Resonance of Liquid Crystals, Spring-Verlag, N.Y., 1994, Chap. 2.

7. R.Y. Dong, Bull of Magn. Reson. 14, 134 (1992); S. Wimperis, J. Magn. Reson. 86, 46 (1990).

8. J.W. Goodby, G.W. Gray, A.J. Leadbetter and M.A. Mazid in "Liquid Crystals of One- and Two- dimensional Order" Eds. W. Helfrich and G. Heppke (Spring-verlag, Berlin Heidelberg, 1980).

Chapter 5

Rotational Dynamics of a Smectogen

Here we present our experimental data in all the mesophases for 5O.7-d_1 and 5O.7-d_4. Figures 10 and 11 show the spectral densities versus the temperature ($T_C - T$) for 5O.7-d_1 and 5O.7-d_4, respectively, at 15.3 and 46 MHz, where T_C is the clear point, *i.e.*, the isotropic liquid-nematic phase transition temperature. We will use the theory outlined in Chap. 2 to discuss the data in "disordered" liquid like phases and the theory described in Chap. 3 to discuss the results obtained from the "ordered" solid-like phases.

5.1 In "Disordered" Liquid-like Phases

For clarity the spectral densities $J_1(\omega_0)$ and $J_2(2\omega_0)$ in the nematic, smectic A and C phases of 5O.7-d_1 and 5O.7-d_4 are plotted in figs. 12 and 13, respectively. As seen from these figures, $J_1(\omega)$ is larger than $J_2(2\omega)$. Both $J_1(\omega)$ and $J_2(2\omega)$ increase with decreasing temperature and show no apparent discontinuties at the $N - S_A$ and $S_A - S_C$ phase transitions. The $J_2(2\omega)$ of both methine and ring deuterons are within experimental errors independent of the Larmor frequency, while their J_1's are frequency dependent. Such frequency dependences have been obtained from deuterated solute diethynyl-benzene (DEB-d_2) dissolved in liquid crystals Merck Phase V [1] and 4O.8 [2]. We found that molecular reorientation alone cannot ac-

count for the different frequency dependences of $J_1(\omega_0)$ and $J_2(2\omega_0)$. Furthermore the frequency dependence in $J_1(\omega_0)$ of the methine deuteron is substantially larger than that of the ring deuterons. These observations lead us to believe that director fluctuations must contribute to $J_1(\omega_0)$ in the studied MHz region. In particular we note in eq. (47) of chap. 2 that contribution of director fluctuations depends on the angular factor $P_2(\cos\theta)$. The θ angle for the methine and ring deuterons are 68° and 60°, respectively. Since the value of $P_2(\cos\theta)$ varies rapidly near the magic angle (54.7°), we anticipate quite different effects on the experimental $J_1(\omega_0)$ of the methine and ring deuterons.

We adopt a model in which both the reorientation/internal motions and director fluctuations are effective relaxation mechanisms. The experimental spectral densities can be calculated using

$$\begin{aligned} J_1^{(i)}(\omega_0) &= J_{1R}^{(i)}(\omega_0) + J_{1DF}^{(i)}(\omega_0) \\ J_2^{(i)}(\omega_0) &= J_{2R}^{(i)}(2\omega_0) \end{aligned} \tag{62}$$

where the subscript R denotes the contribution from molecular rotation and the corresponding spectral densities can be evaluated using either the third rate model or Nordio's model. We have tried both models of molecular reorientation and found that the third rate model in conjunction with director fluctuations can successfully interpret the spectral densities measured in the present study. Thus the analyses based on the third rate model will be given first.

In the third rate model, there are three model parameters D_α, D_β and D_γ in

the correlation times ($p = 0$) given by eq. (44) of Chap. 2. To evaluate $a^{(j)}_{m_L m_M}$, $b^{(j)}_{m_L m_M}$ and $C_{m_L m_M}$ coefficients at each temperature, the nematic order parameter $\langle P_2 \rangle$ is first calculated from the quadrupolar splitting of the methine deuteron using eq. (29) of Chap. 2 with the assumption of zero $(S_{xx} - S_{yy})$

$$\delta\nu_Q = \frac{3}{4} q_{CD} (3\cos\theta^2_{M,Q} - 1)\langle P_2 \rangle \tag{63}$$

where $q_{CD} = 185$ kHz and $\theta_{M,Q} = 68°$ [3]. This is an approximation as chain deuterated 5O.7 sample is unavailable at present. Ideally one must consider all possible configurations [4,5] of the molecule in order to calculate the orientational order of an "average" conformer. $a^{(j)}_{m_L m_M}$, $b^{(j)}_{m_L m_M}$ and $C_{m_L m_M}$ are obtained from the $\langle P_2 \rangle$ values according to table I of Ref. 6. Two additional model parameters D_R and a_{DF} are needed to account for the internal ring rotation and director fluctuations, respectively. At each temperature, there are eight measured spectral densities (two J_1's and two J_2's at each frequency) from which five model parameters can in principle be determined. For simplicity, we will neglect for the moment the small negative cross term in eq. (47) in chap. 2. In deriving the model parameters, smoothed lines through the data in figures 12 and 13 were used. Given a set of model parameters, we can compute the theoretical spectral densities of the methine and ring deuterons at each Larmor frequency using eqs. (39), (45) and (47). A minimization routine (Amoeba) [7] was used to search for best values of the model parameters by minimizing the sum squared error F

$$F = \sum_{\omega_0} \sum_{i} \sum_{m_L} \left[J^{(i)Calc}_{m_L}(m_L\omega_0) - J^{(i)Expt}_{m_L}(m_L\omega_0) \right]^2 \tag{64}$$

The fitting quality factor Q is given by the percentage mean-squared deviation.

$$Q = 100F / \sum_{\omega_0} \sum_{i} \sum_{m_L} \left[J_{m_L}^{(i)Expt}(m_L\omega_0) \right]^2 \tag{65}$$

Our attempt on minimizing F by varying D_α, D_β, D_γ, D_R and a_{DF} was met with limited success. We found that a_{DF} remains more or less constant (with an average value of $1.45 \times 10^6 s^{-3/2}$) over the temperature range of 25°C and the temperature dependences of all the diffusion constants except D_β obey a thermally activated behaviour. In other words, D_β decreases with increasing temperature, which seems quite unphysical. Thus, the four spectral densities (two J_1's and two J_2's) measured at two frequencies are still insufficient to yield physical results for all the unknown model parameters. To reduce the number of unknowns, we may assume $D_\alpha = D_\beta = D$ as a first approximation. By repeating the above analyses, we found that D, D_γ and D_R now show expected temperature behaviours and a_{DF} is essentially constant at the above value of $1.45 \times 10^6 s^{-3/2}$. It would seem reasonable to fix a_{DF} and to allow the four diffusion constants to vary at each temperature. We repeated the analyses with slightly different a_{DF} values and found that a value of $1.38 \times 10^6 s^{-3/2}$ works over the studied temperature range except within few degrees of T_c where the a_{DF} value decreases to $1.25 \times 10^6 s^{-3/2}$ at T_c. Using Noack's notation, A_{DF} is defined by [8]

$$A_{DF} = [P_2(\cos\theta)]^2 a_{DF} / \sqrt{2\pi} \tag{66}$$

The corresponding A_{DF} value for the ring deuterons is 8594 $s^{-3/2}$ (7813 $s^{-3/2}$ at T_c). No A_{DF} value has been obtained for 5O.7 from NMR field-cycling experiments

and a direct comparison with the above A_{DF} values is not possible. Since A_{DF} is proportional to the square of the spectral splitting (e.g. dipolar splitting for a pair of ring protons or quadrupolar splitting for a ring deuteron), one may estimate the A_{DF} value of the ring deuterons in 1O.4 to be close to 7940 $s^{-3/2}$. This is based on the results from the ring protons [8] at $T_c - T = 10°C$ in 1O.4-d_{13}. Therefore the A_{DF} values used here appear to be reasonable. In table 4, we summarize the results of our four-parameter fit of the experimental spectral densities to the third rate model of molecular reorientation. Theoretical spectral densities for the two deuterated sites are also shown in figures 12 and 13 by solid and dashed curves for $J_1(\omega)$ and $J_2(2\omega)$, respectively. We found that the agreement between experiment and theory is rather good in the N, S_A and S_C phases of 5O.7. It is important to note that director fluctuations make a large contribution to the observed J_1's. For example, in the middle of the N phase director fluctuations account for about 60% and 47.5% of the experimental methine $J_1(\omega_0)$ at 15.3 and 46 MHz, respectively, and about 21% and 13% of the experimental ring $J_1(\omega_0)$ at these frequencies. These percentages decrease in the smectic phases as contribution to J_1 due to molecular reorientation increases with decreasing temperature. We plot the rotational diffusion constants versus the reciprocal temperature in figure 14. The $\gamma-$motion appears to noticeably show a pre-transitional behaviour at T_c. All the diffusion constants increase with increasing temperature except close to T_c. As may be seen in figures 12 and 13, the smoothed lines from which the spectral density data were obtained for model calculations are less reliable near T_c. The apparent pre-transitional behaviours may

be deceptive because of the larger uncertainty in the derived model parameters than what the error bars indicate in figure 14. The error bars are estimated by varying the model parameter under consideration while keeping the other three model parameters identical to those for minimum F, to give a doubling in the F value. The activation energy E_a for the $\alpha-, \beta-$ and ring motions is 25 kJ/mol, 40 kJ/mol and 120 kJ/mol, respectively. The apparent E_a for the $\gamma-$motion is ca. 21 kJ/mol. We found that the γ-motion is fastest, followed by the α-motion and then the β-motion. The rate of aniline ring rotation is comparable to the $\alpha-$, $\beta-$motions in the nematic phase and becomes slower in the smectic A and C phases. The high activation energy for D_R may be an indication that ring flips have become hindered or even frozen in the S_B phase. Another possibility is that D_R has the largest error bar, especially at low temperatures where its small values make it unimportant in comparison with the correlation times of molecular reorientation. We have tried to include the negative cross term in eq. (47) keeping the same a_{DF} values and found that the Q-factors at several temperatures deteriorate by at least a factor of ten. Furthermore the derived values of D_β and D_γ decrease with increasing temperature. Thus the cross term is either inappropriate or the assumption of 200 MHz for the cutoff frequency is incorrect for 5O.7.

Finally, we like to comment on Nordio's model. In a recent study of internal dynamics [4] in 1O.4-d_{13}, Nordio's model is found to be inferior in comparison with the third rate model. A similar case can be made here except the evidence is not as compelling. Since the contribution from director fluctuations should be same

regardless of which model of molecular reorientation is used, the same a_{DF} values are used in conjunction with Nordio's model. There are two model parameters $D_{||}$ and $D_{\perp}$ which appear in the correlation times (eq. (41)) plus D_R for internal ring rotations. A three-parameter fit of the experimental methine and ring data to Nordio's model produces similar Q's as in table 4. The results are summarized in table 5. Although the Q-factors are comparable to those for the third rate model, the prediction that the tumbling motion is faster than the spinning motion of the molecule ($D_{\perp} > D_{||}$) for the entire studied temperature range, is unlikely to be correct for a rodlike molecule like 5O.7. Furthermore, $D_{\perp}$ exhibits a wrong temperature dependence. We therefore have to rule out Nordio's model as acceptable for 5O.7. It would be useful to have chain deuterated 5O.7 to further support this finding.

In conclusion, director fluctuations are important in relaxing the deuteron spins of 5O.7 in the nematic, smectic A and C phases. This is apparently not the case [4] in 1O.4 at 15.3 MHz because of its lower clearing temperature. For example, at $T_c - T = 25°C$, the J_1 of methine deuteron in 1O.4 is a factor of four larger than that of 5O.7. Thus the contribution from molecular reorientation is dominant in 1O.4, at least at temperatures not close to T_c. Both 1O.4 and 5O.7 appear to favour the third rate model of molecular reorientation.

5.2 In "Ordered" Solid-like Phases

It is apparent in figures 10 and 11 that there are discontinuities in $J_1(\omega)$ and

$J_2(2\omega)$ at the S_C-S_B phase transition. Figures 15 and 16 present the spectral densities versus $T_C - T$ in the S_B and S_G phases of 5O.7$-d_1$ and 5O.7$-d_4$, respectively. Over the whole range of smectic B and G phases, both $J_1(\omega)$ and $J_2(2\omega)$ are frequency dependent and change smoothly through $S_B - S_G$ phase transition for the methine and ring deuterons. The J_1/J_2 ratio is near 1 for the methine deuteron and is much larger for the ring deuterons. Furthermore, the frequency dependences of spectral densities are more pronounced for the ring deuterons. Since the internal ring rotation in the smectic C phase has substantially slowed down, it is reasonable to assume that ring rotation is frozen ($D_R = 0$) in the smectic B and G phases of 5O.7. Then the difference in spectral densities between the methine deuteron and ring deuterons must due exclusively to the geometric factors of C-D bond of these two kinds of deuterons. To account for the frequency dependences of $J_1(\omega)$ and $J_2(2\omega)$, some restricted motional mechanisms must be invoked. Biased $\gamma-$motions in "ordered" smectic phases have been detected by ^{13}C NMR and ^{14}N NQR [9]. It is clear that director fluctuations are unimportant in these phases.

Using the restricted libration model (eq. (53)) to fit the spectral density data in S_B and S_G phases, there are four model parameters D_α, D_β, D_ϕ and ϕ_0. A computer program is written using Amoeba to minimize the F. It is found that the D_β values are very small ($\sim\ 10^4\ s^{-1}$) compared with those of the D_α ($\sim\ 10^6\ s^{-1}$) and D_ϕ ($\sim\ 10^9\ s^{-1}$). Furthermore, putting $D_\beta = 0$ makes trivial difference on the minimized F value. Theoretical spectral densities (solid and dashed lines for $J_1(\omega_0)$ and $J_2(2\omega_0)$, respectively) are shown in figures 15 and 16. It is seen that the agree-

ment between the experiment and theory is quite good, especially in the S_B phase. The fits in the S_G phase show some systematic deviations but still within the experimental errors except at very low temperatures, where S/N ratio is really poor. Furthermore, the short T_1 values at the low temperature end of the S_G phase, *c.a.* 3 ms, have made these measurements difficult and less reliable. We note that for the methine deuteron, the experimental J_1/J_2 ratios at 46 MHz are slightly bigger than 1, whereas the corresponding theoretical ratios are slightly less than 1. Although the deviation is within the experimental errors, further accurate experimental data are needed for better fitting. The rotational diffusion constants versus the reciprocal temperature are plotted in figure 17, D_ϕ describes biased libration about the long molecular axis and shows the normal temperature behaviour, *i.e.* it decreases with decreasing temperature. We notice that the D_ϕ value in the S_B phase near the $S_C - S_B$ phase transition is *c.a.* $3.5\times10^9\ s^{-1}$, while its analogous D_γ value in the S_C phase [Fig. (14)] near $S_C - S_B$ phase transition is *c.a.* 4.4×10^9/s. Thus the diffusion constant for the $\gamma-$motion does not show a drastic change at this phase transition. However, the activation energy E_a for D_ϕ (*c.a.* 42 KJ/mol) is higher than that of D_γ (*c.a.* 21 KJ/mol). The apex angle ϕ_0 varies slightly around 200° in smectic B and G phases, so the libration angular amplitude is about ±100°. It seems that the ϕ_0 decreases with decreasing temperature according to figure 18, which is quite reasonable because the lower the temperature, the more biased the $\gamma-$motion is. The molecular motion towards the director is strongly hindered ($D_\beta \sim 0$) due to the close hexagonal packing within each layer in smectic B and G phases. The

$\alpha-$motion is much slower than the biased libration around the molecular z-axis. The D_α values in these "ordered" smectic phases are more or less the same, *c.a.* $3\times10^6\ s^{-1}$. Because of the small D_α values, the $\alpha-$motion is very slow and is hard to be determined in the present study. This could explain the apprent increase of D_α with decreasing temperature in the S_B phase which is unphysical.

Finally, we like to comment on biaxial phases. Generally, for cylindrical symmetric molecules, as long as the director is parallel the external field, the biaxial terms do not contribute to the spectral densities (Eqs. (59-60)). Smectic C phase was probably the first mesophase to be recognized as biaxial. When treating spin relaxation in smectic C phases [10], it was assumed that effects of phase biaxiality are small and may be neglected. It is already known that the director is aligned by the external magnetic field in smectic C phases [11]. There are no discontinuities at the $S_A - S_C$ and at the $S_B - S_G$ phase transitions in our spectral density data for 5O.7. The results of Berggren *et al.* [12] were based on Nordio's diffusion model, which could be applied to the S_C phase. One can extend their results for the third-rate model in a manner described by Vold and Vold [13]. According to equations (59−60), the biaxial terms vanish in the expressions of spectral densities when the director is parallel to the external field. It is not surprising to see that the spectral densities vary smoothly through $S_B - S_G$ phase transition, since the director is aligned while the layers are tilted in the S_G phase of 5O.7 [14].

In conclusion, the uniaxial restricted model appears to work in both S_B and S_G phases of 5O.7. Perhaps the slow $\alpha-$ motion needs further inspection, especially in

the S_B phase. To further study biaxial phases, angular dependent relaxation rates must be carried out.

Table 4

Results of four-parameter minimization of sum squared error between experimental spectral density data to the third rate model of molecular reorientation. Director fluctuations (a_{DF}) contribute to J_1's whose values are fixed.

T(°C)	$\langle P_2 \rangle$	$a_{DF}(s^{-3/2})$	$D_\alpha(s^{-1})$	$D_\beta(s^{-1})$	$D_\gamma(s^{-1})$	$D_R(s^{-1})$	Q
76.5	0.38	1.25×10^6	2.14×10^9	1.13×10^9	6.47×10^9	2.07×10^9	0.005
74.5	0.44	1.30×10^6	2.22×10^9	1.16×10^9	6.45×10^9	1.61×10^9	0.005
72.5	0.49	1.38×10^6	2.05×10^9	1.14×10^9	7.25×10^9	1.02×10^9	0.026
70.0	0.53	1.38×10^6	2.09×10^9	0.91×10^9	7.49×10^9	0.89×10^9	0.040
67.5	0.57	1.38×10^6	1.96×10^9	0.82×10^9	7.39×10^9	0.67×10^9	0.018
62.5	0.67	1.38×10^6	1.63×10^9	0.68×10^9	6.87×10^9	0.44×10^9	0.005
57.5	0.74	1.38×10^6	1.39×10^9	0.58×10^9	5.80×10^9	0.17×10^9	0.049
52.5	0.78	1.38×10^6	1.18×10^9	0.45×10^9	4.71×10^9	0.09×10^9	0.065

Table 5

Results of three-parameter minimization of sum squared error between experimental spectral density data to Nordio's model. a_{DF} values are identical to those given in table 4.

T($^\circ C$)	$D_\parallel(s^{-1})$	$D_\perp(s^{-1})$	$D_R(s^{-1})$	Q
77.5	2.86×10^9	2.91×10^9	2.27×10^9	0.025
72.5	2.40×10^9	4.54×10^9	1.85×10^9	0.048
67.5	2.00×10^9	5.08×10^9	1.60×10^9	0.050
62.5	1.23×10^9	5.75×10^9	1.20×10^9	0.041
57.5	0.70×10^8	5.69×10^9	0.57×10^9	0.067
52.5	0.40×10^8	5.21×10^9	0.26×10^9	0.120

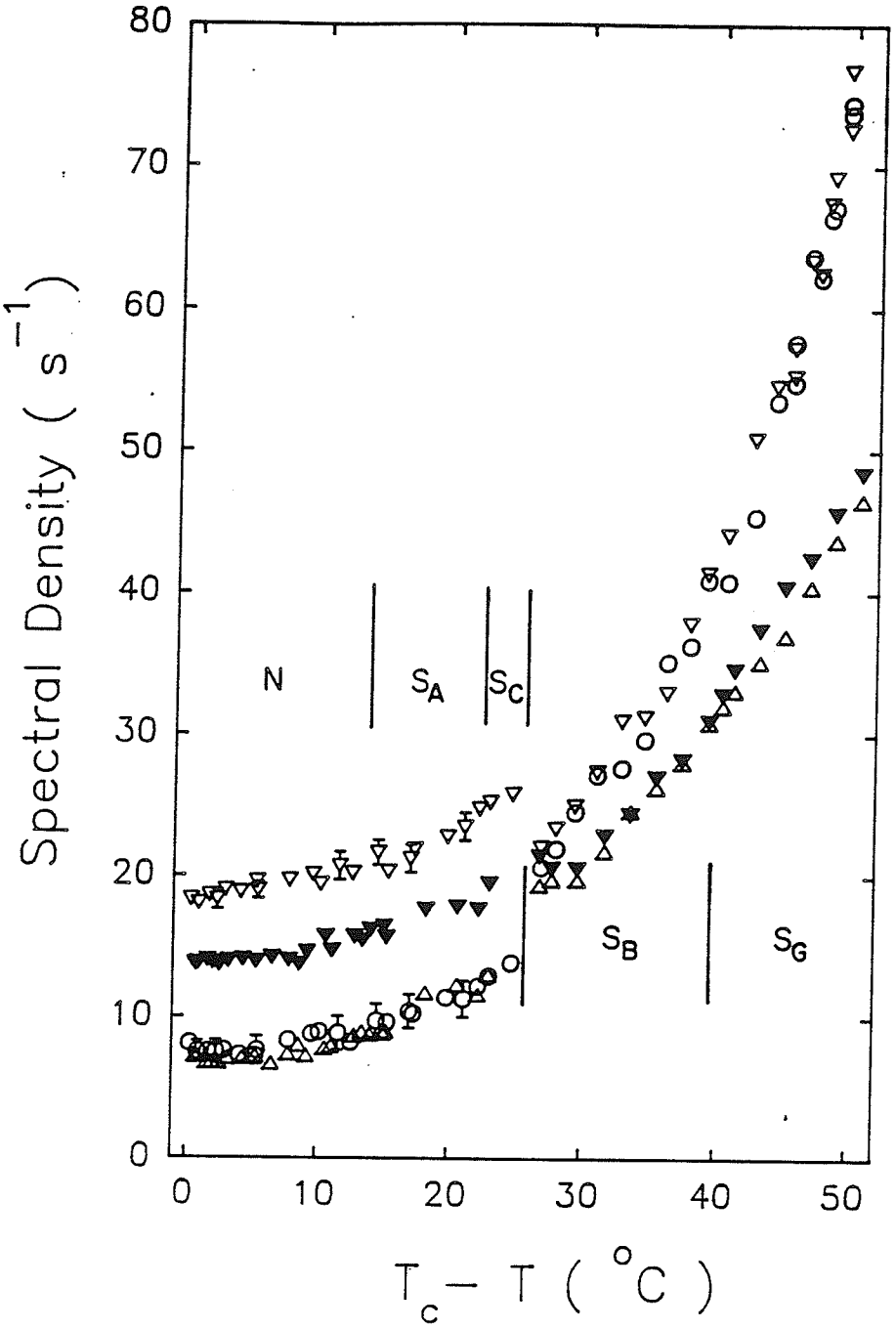

Figure 10 Plots of spectral densities versus $T_c - T$ of 5O.7$-d_1$. $\bigtriangledown$ and $\bigcirc$ denote $J_1(\omega_0)$ and $J_2(2\omega_0)$ in 15.3 MHz, respectively. $\blacktriangledown$ and $\bigtriangleup$ denote $J_1(\omega_0)$ and $J_2(2\omega_0)$ in 46 MHz, respectively.

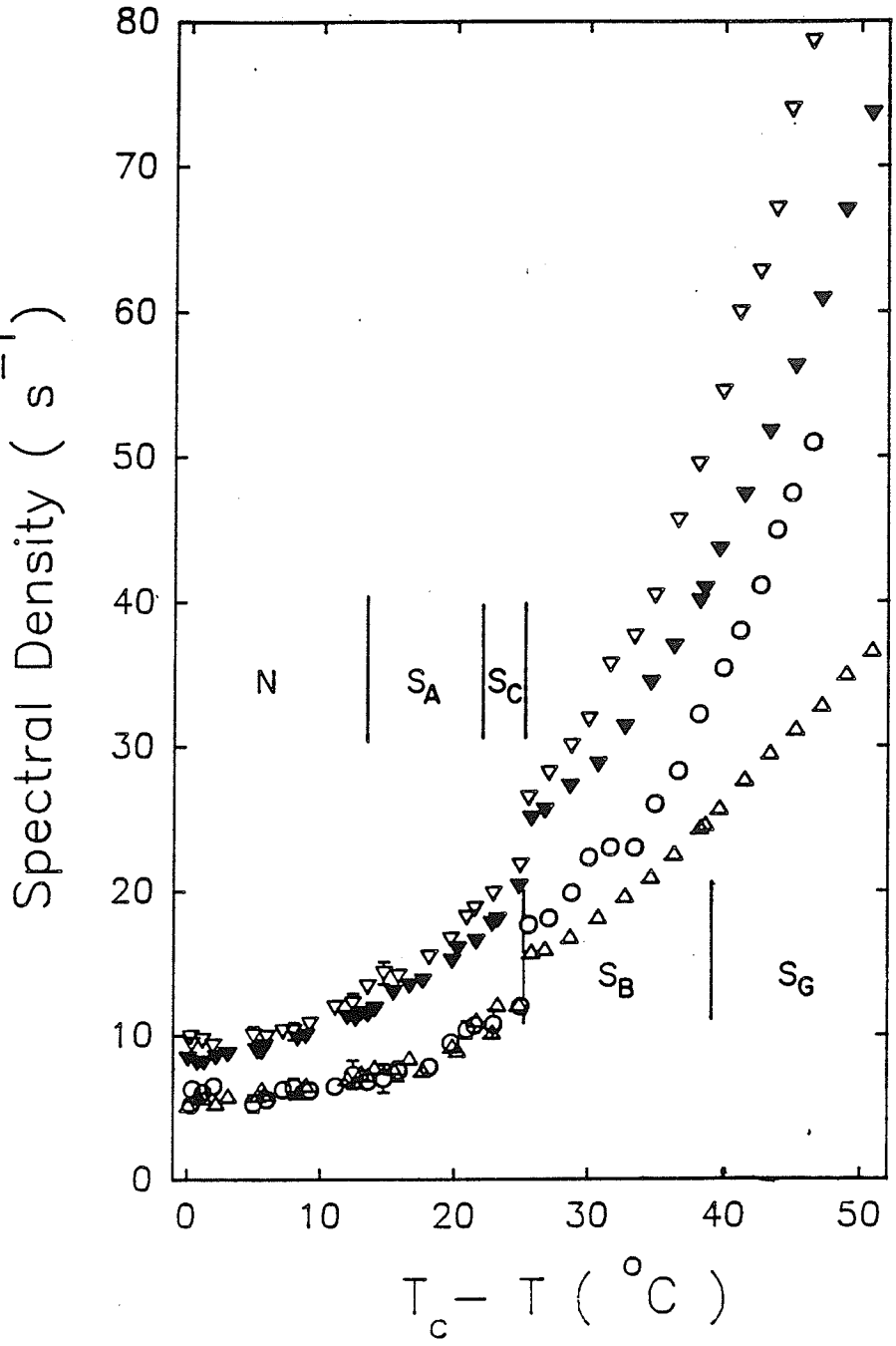

Figure 11 Plots of spectral densities versus $T_c - T$ of 5O.7$-d_4$. $\bigtriangledown$ and $\bigcirc$ denote $J_1(\omega_0)$ and $J_2(2\omega_0)$ in 15.3 MHz, respectively. $\blacktriangledown$ and $\bigtriangleup$ denote $J_1(\omega_0)$ and $J_2(2\omega_0)$ in 46 MHz, respectively.

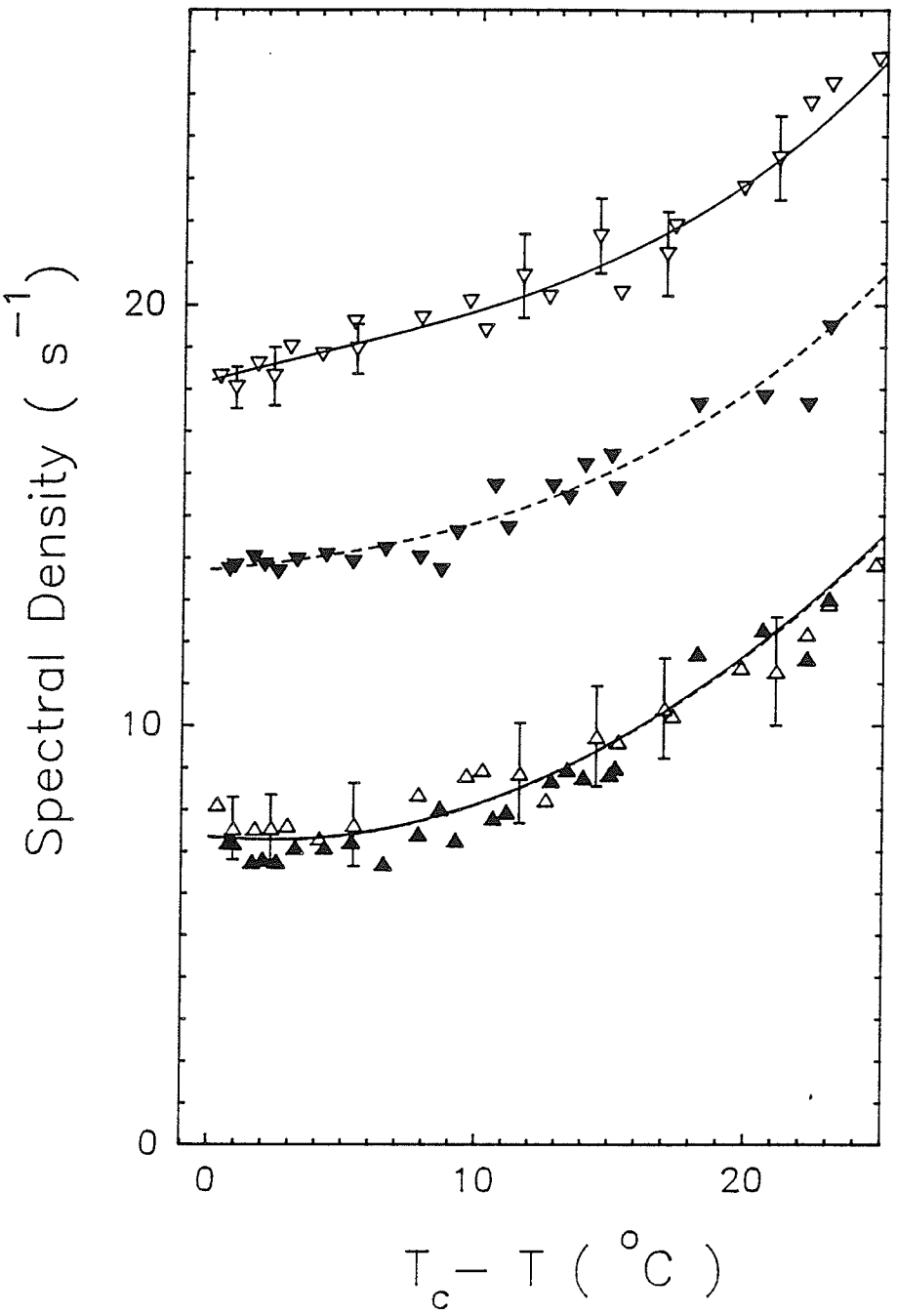

Figure 12 Plots of spectral densities versus $T_c - T$ in the nematic, smectic A and C phases of 5O.7-d_1. $\bigtriangledown$ and $\bigtriangleup$ denote $J_1(\omega_0)$ and $J_2(2\omega_0)$, respectively. Open symbols denote data at 15.3 MHz, while closed symbols at 46.05 MHz. Solid and dashed curves are theoretical spectral densities based on the third rate model of molecular reorientation and director fluctuations.

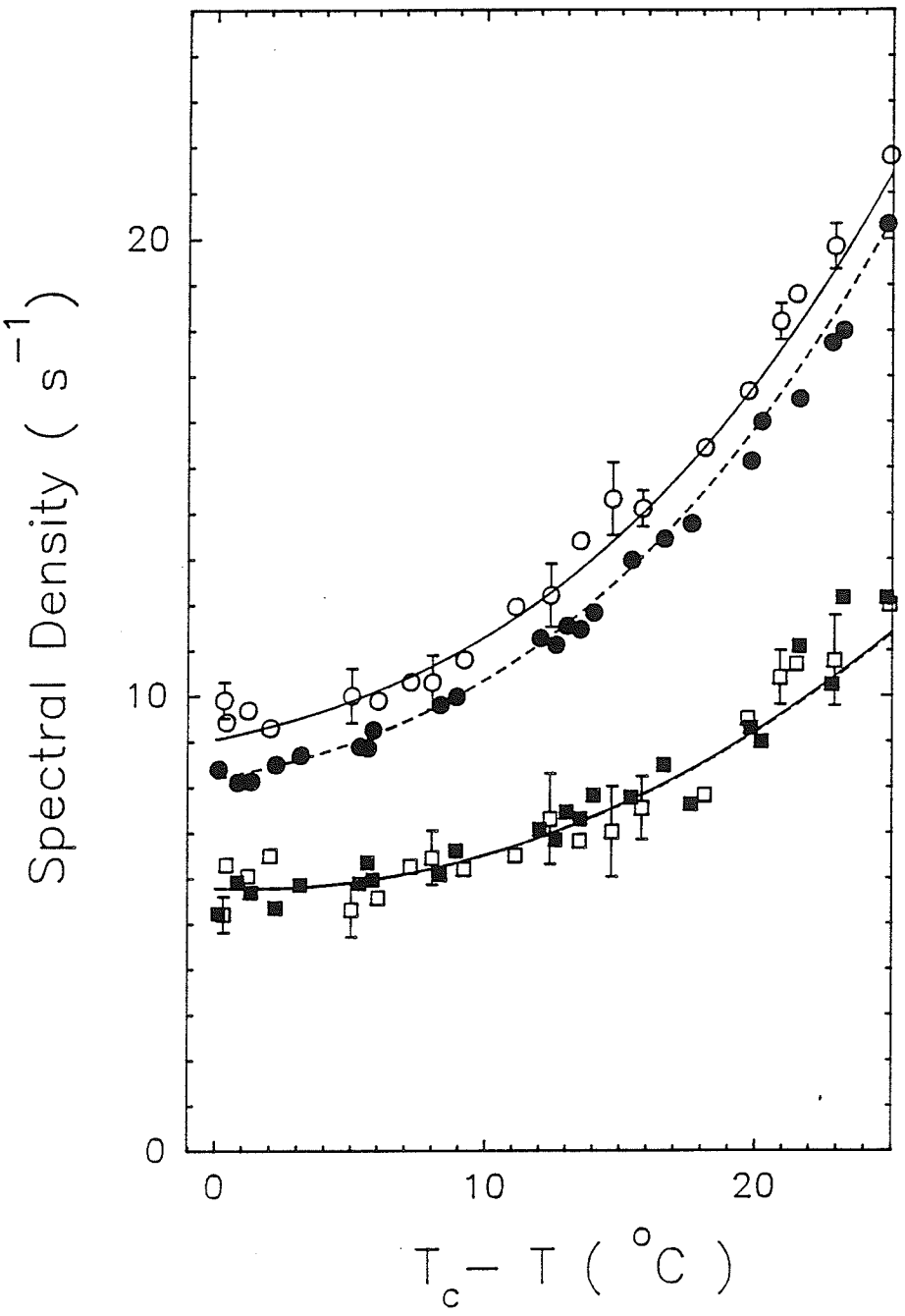

Figure 13 Plots of spectral densities versus $T_c - T$ in the nematic, smectic A and C phases of 5O.7-d_4. ○ and □ denote $J_1(\omega_0)$ and $J_2(\omega_0)$, respectively. Open symbols denote data at 15.3 MHz, while closed symbols at 46.05 MHz. Solid and dashed curves are theoretical spectral densities based on the third rate model of molecular reorientation and director fluctuations.

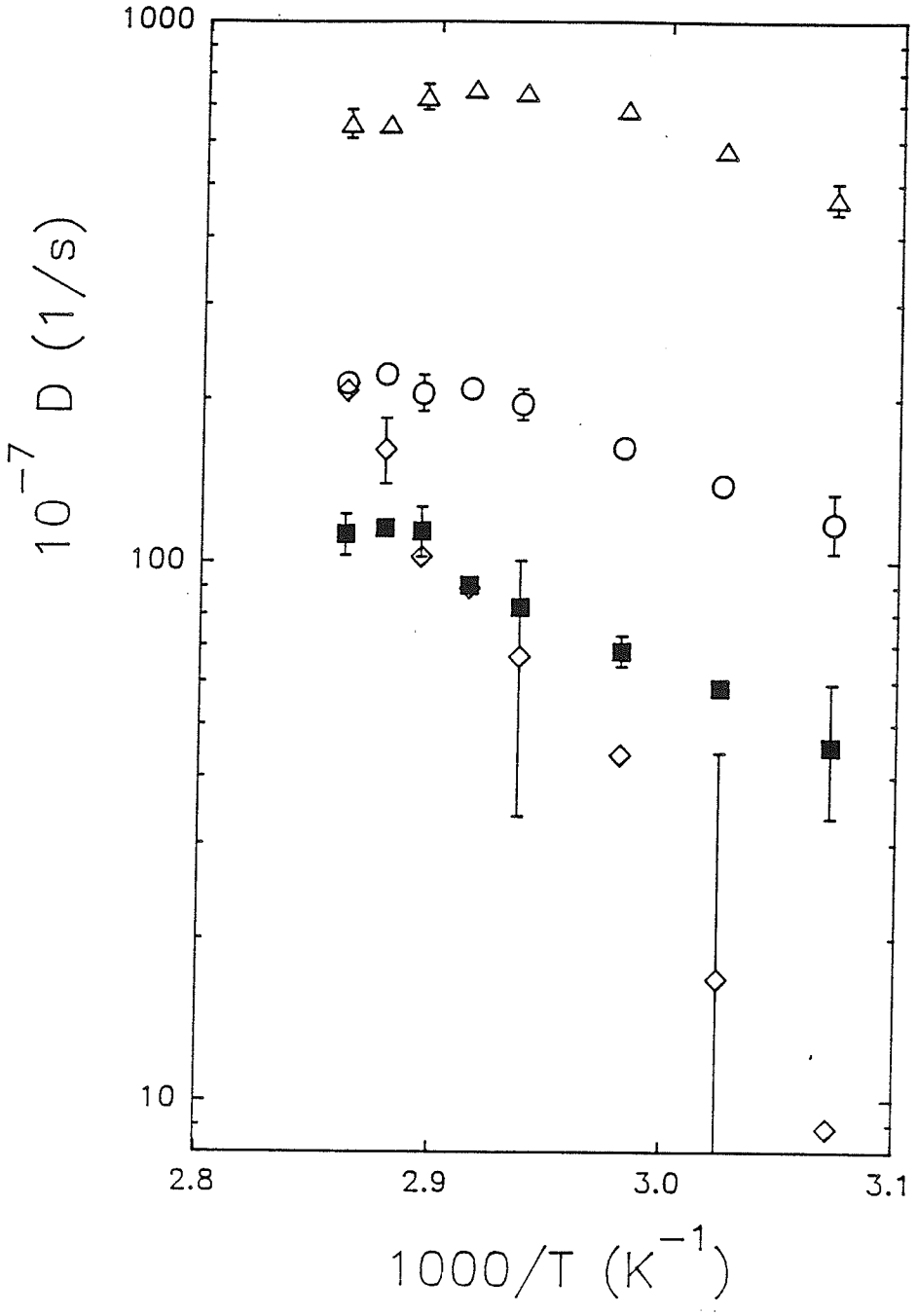

Figure 14 Plots of rotational diffusion constants D_α (○), D_β (■), D_γ(△) and D_R (◇) versus the reciprocal temperature in "disordered" liquid-like phases. Error bars are estimated by doubling the F' value obtained in the minimization (see text).

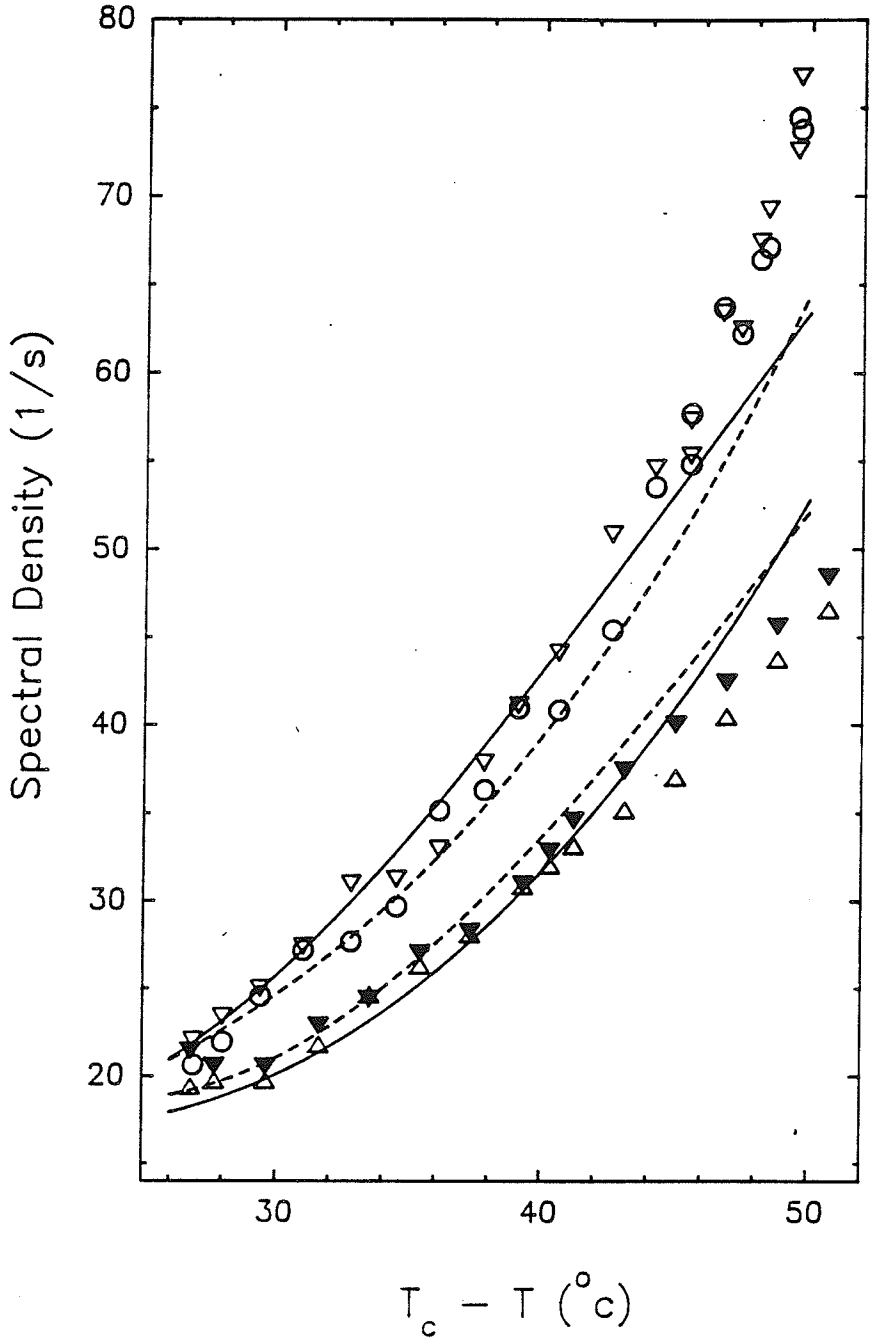

Figure 15 Plots of spectral densities versus $T_c - T$ in smectic B and G phases of 5O.7$-d_1$. ∇ and $\bigcirc$ denote $J_1(\omega_0)$ and $J_2(2\omega_0)$ in 15.3 MHz, respectively. $\blacktriangledown$ and $\triangle$ denote $J_1(\omega_0)$ and $J_2(2\omega_0)$ in 46 MHz, respectively. Solid and dashed curves denote theoretical $J_1(\omega_0)$ and $J_2(2\omega_0)$, respectively, based on the restricted libration model of molecular reorientation.

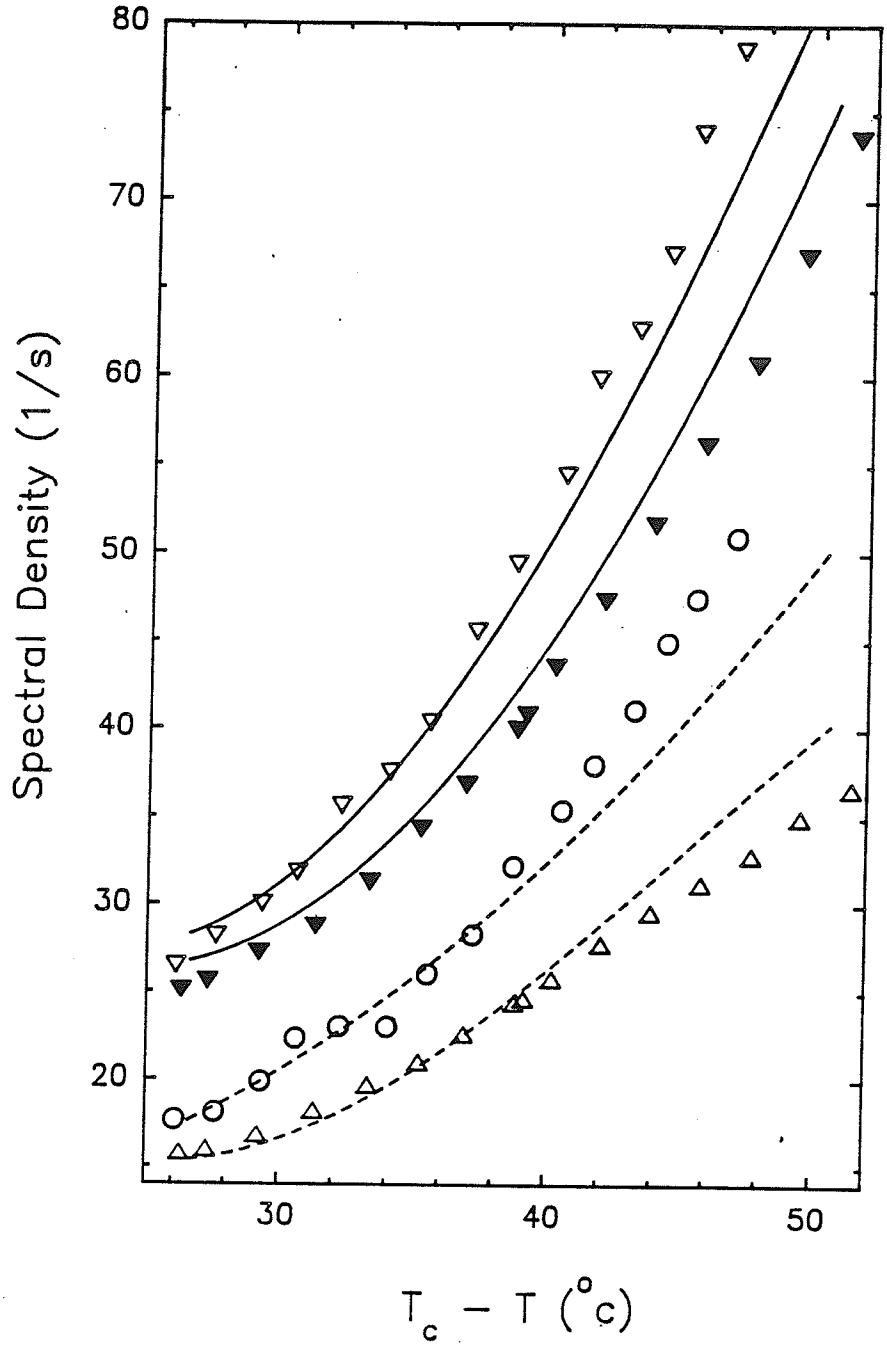

Figure 16 Plots of spectral densities versus $T_c - T$ in smectic B and G phases of 5O.7$-d_4$. $\bigtriangledown$ and $\bigcirc$ denote $J_1(\omega_0)$ and $J_2(2\omega_0)$ in 15.3 MHz, respectively. $\blacktriangledown$ and $\bigtriangleup$ denote $J_1(\omega_0)$ and $J_2(2\omega_0)$ in 46 MHz, respectively. Solid and dashed curves denote theoretical $J_1(\omega_0)$ and $J_2(2\omega_0)$, respectively, based on the restricted libration model of molecular reorientation.

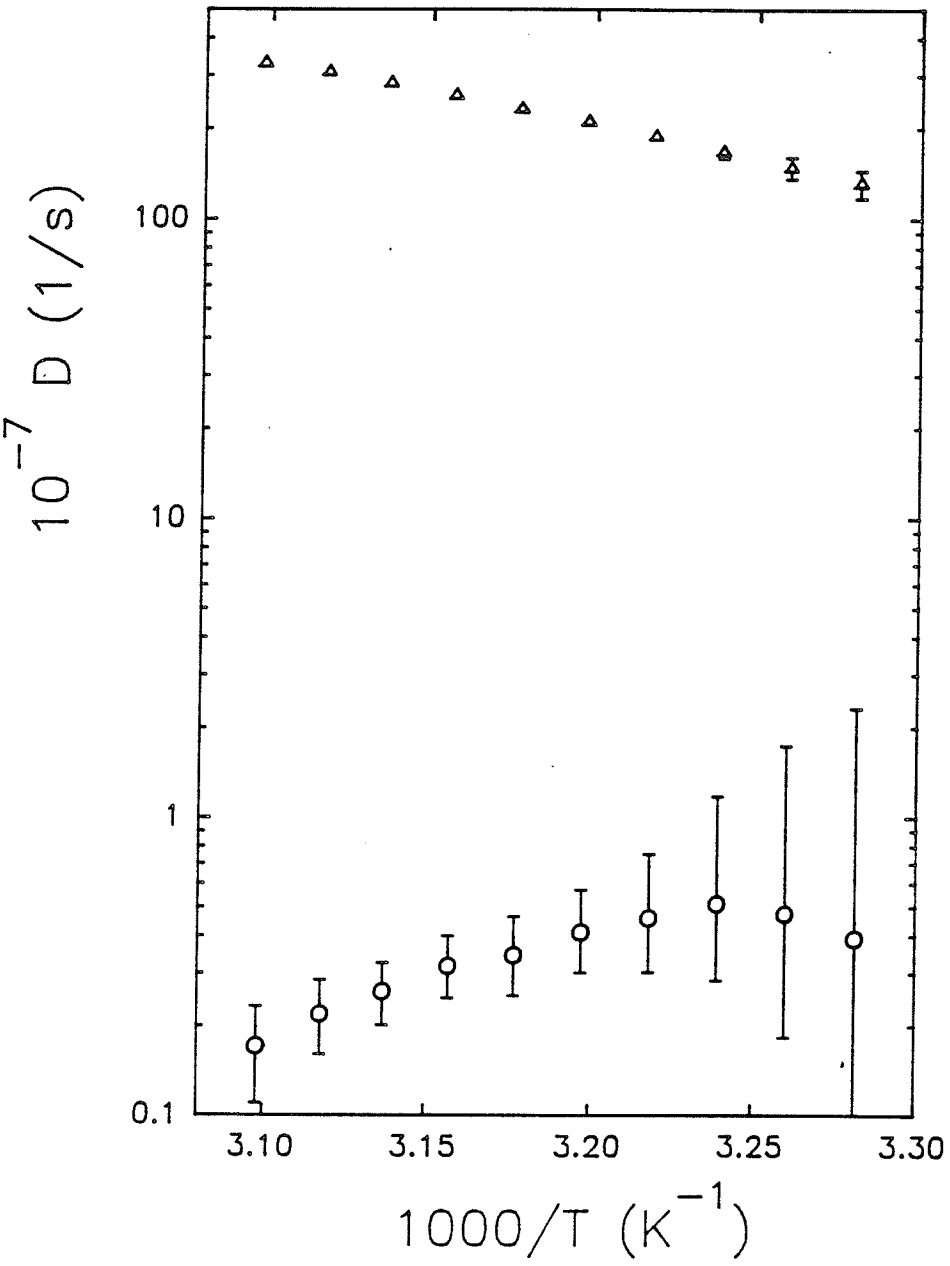

Figure 17 Plots of rotational diffusion constants D_α (○) and D_ϕ(△) versus the reciprocal temperature in "ordered" solid-like phases. Error bars are estimated by doubling the F value obtained in the minimization (see text).

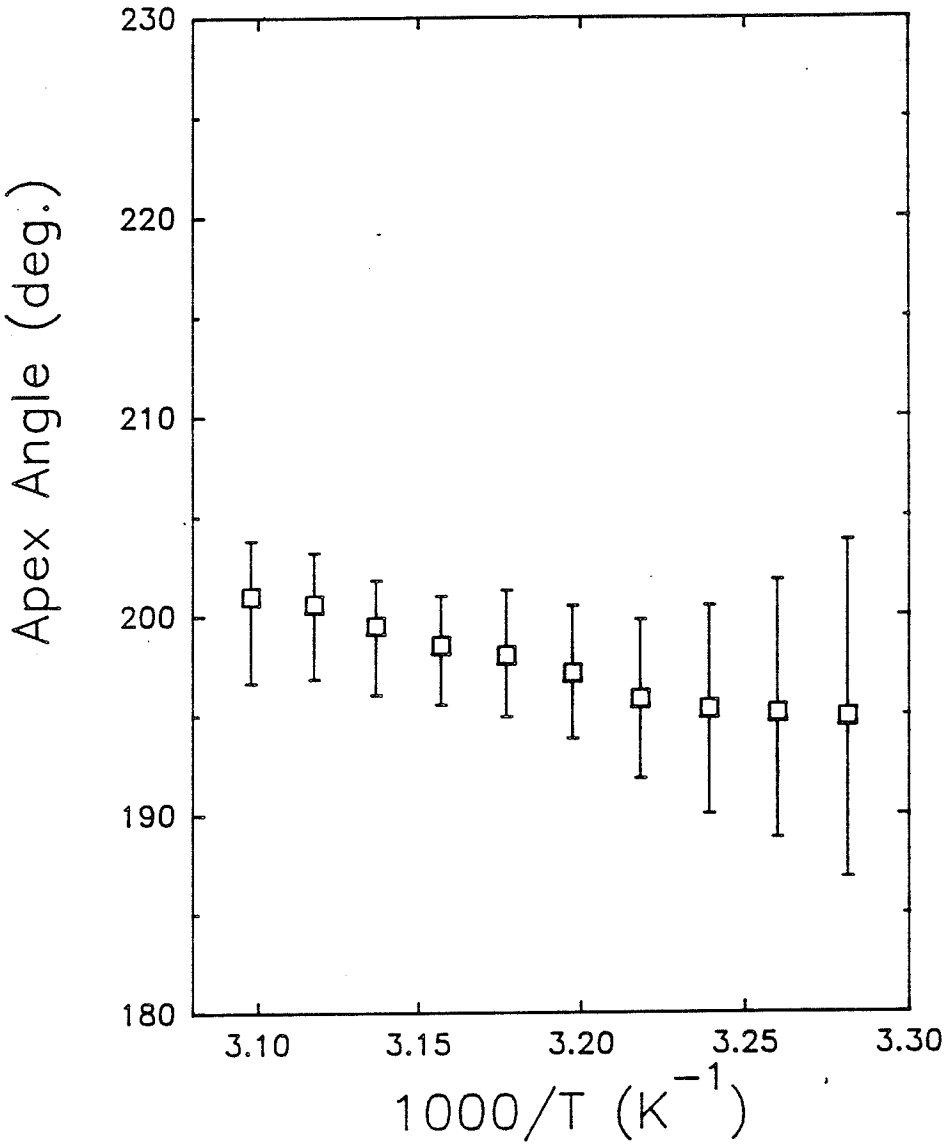

Figure 18 Plots of apex angle of molecular libration ϕ_0 (□) versus the reciprocal temperature in "ordered" solid-like phases. Error bars are estimated by doubling the F value obtained in the minimization (see text).

References

1. W.H. Dickerson, R.R. Vold and R.L. Vold, J. Phys. Chem. 87, 166 (1983).

2. L.S. Selwyn, R.R. Vold and R.L. Vold, Mol. Phys. 55, 287 (1985).

3. R.Y. Dong, Liq. Cryst. 4, 505 (1989).

4. R.Y. Dong, L. Friesen, and G.M. Richards, Mol. Phys., 1994, to be published.

5. J.W. Emsley, G.R. Luckhurst and C.P. Stockley, Proc. R. Soc. Lond. A 381, 117 (1982).

6. R.R. Vold and R.L. Vold, J. Chem. Phys. 88, 1443 (1988).

7. W.H. Press, B.P. Flannery, S.A. Teukolsky and W.T. Vetterling, "Numerical Recipes", (Cambridge University, Cambridge, U.K., 1986).

8. F. Noack, M. Notter, and W. Weiss, Liq. Cryst. 3, 907 (1988); K.H. Schweikert and F. Noack, Mol. Cryst. Liq. Cryst. 212, 33 (1992).

9. R. Blinc, J. Dolinsek, M. Luzar, and J. Selinger, Liq. Cryst. 3, 663, (1988).

10. R.Y. Dong, 1986, Mol. Cryst. Liq. Cryst. 141, 349.

11. Meiboom S., and Luz Z., 1973, Mol. Cryst. Liq. Cryst. 22, 143; Wise R.A., Smith D.H. and Doane J.W., 1973, Phys. Rev. A 7, 1366.

12. Berggren, E., Tarroni, R. and Zannoni, C., 1993, J. Chem. Phys. 99, 6180.

13. R.R. Vold, and R.L. vold, J. Chem. Phys. 88 (2), 1443, (1988).

14. M.J. Vaz, Z. Yaniv, R.Y. Dong, and J.W. Doane, J. Magn. Reson. 62, 461, (1985).

Chapter 6

Brief Summary

Nuclear spin relaxation measurements can be used to study the molecular dynamics in liquid crystals. The present deuterium NMR study of 5O.7 shows that molecules involve quite different dynamical mechanisms in "disordered" liquid-like phases from those in "ordered" solid-like phases. In the "disordered" liquid-like phases (N, S_A and S_C), the molecular reorientation and director fluctuations are responsible for the observed spectral densities. The contribution to J_1 due to director fluctuations has a characteristic $\omega^{-1/2}$ dependence. By modeling the experimental data, the third-rate model is appropriate in describing molecular rotations whereas Nordio's model is not. The γ-motion is fastest, followed by the α-motion and β-motion. In addition to molecular reorientation, ring rotation about the para-axis of a phenyl ring should be taken into account. Internal rotations in the chains are not dealt with in the present study. In the "ordered" solid-like phases (S_B and S_G), the γ-motion is founded to be restricted within an apex angle ϕ_0. The ring rotation is quenched, the β-motion is strongly hindered and the α-motion becomes much slower due to hexagonal close packings of molecules within each layer. In biaxial phases, spectral densities show phase biaxiality only if the director is oriented away from the external field. An important implication is that future study of phase biaxiality should concentrate on the angular dependences of the spectral densities.

Appendix A

Rotations, Euler Angles and Wigner Rotation Matrices

There are two primary reasons for looking at rotations in NMR of liquid crystals. First, rotational motion of the spin-bearing molecules determines in part relaxation behaviour of the spin system. Second, one or more rf pulse(s) in NMR experiments has the effect of rotating the spin angular momentum of the spin system. Therefore, we need to deal with spatial rotations of the spin system and with spin rotations. The connection between rotations and angular momentum ($\vec{J}$) is expressed by a rotation operator

$$R_n(\Omega) = \exp[-i\Omega\vec{J} \bullet \hat{n}] \tag{67}$$

where $\hat{n}$ is a unit vector directed along an axis n. The operator represents a rotation about the n axis by angle Ω. The derivation of eq. (67) can be found in most quantum mechanics texts. It can be shown that the rotation operator is unitary (*i.e.* $R^{-1} = R^{\dagger}$). In coordinate system transformation, a positive rotation of angle Ω about an axis n is to rotate the two perpendicular axes by the right-hand rule (*i.e.* with the thumb pointing along the positive n axis, the perpendicular plane moves in the direction of the fingers wrapped around the axis of rotation). In other words, when looking in the direction of the rotation axis, a positive rotation means that the remaining two axes rotate clockwise. Consider a coodinate system transformation that takes one set of axes (X, Y, Z) into another set (x, y, z) which shares the same

origin. This change can always be obtained by three successive rotations, *i.e.*

$$R(\alpha,\beta,\gamma) \;=\; R_z(\gamma)R_N(\beta)R_Z(\alpha) \tag{68}$$

where the Euler angles ($\Omega \equiv (\alpha,\beta,\gamma)$) that produce the coordinate system transformation are given in figure 3 in Chapter 1. From the figure, we see that first we rotate by angle α about the Z axis ($R_z(\alpha)$), then rotate by angle β about the nodal line N, and finally about the z axis by angle γ. An equivalent rotational operator using rotations about the original axis system is

$$R(\alpha,\beta,\gamma) \;=\; R_Z(\alpha)R_Y(\beta)R_Z(\gamma) \tag{69}$$

Note the order reversal from eq. (68) of the rotations with angles α and γ. We will use the Euler angles and the transformation of coordinate axes according to eq. (68). For example, our "original X, Y, Z frame" to "final x, y, z frame" can be from the laboratory frame to the principal axes of an interaction tensor (in its principal axis system, we use $\rho_{J,m}$ to denote an irreducible spherical tensor). When a rotation of a coordinate system is performed (by a rotational operator R), the irreducible spherical tensor component $T_{J,m}$ is transformed into a linear combination of the set of $2J+1$ operators $T_{J,m'}$

$$\begin{aligned} \rho_{J,m} \;&=\; R(\alpha,\beta,\gamma)\; T_{J,m} R^{-1}(\alpha,\beta,\gamma) \\ &=\; \sum_{m'} D^{J}_{m',m}\,(\alpha,\beta,\gamma)\; T_{J,m'} \end{aligned} \tag{70}$$

where $D^{J}_{m',m}(\Omega)$ denote Wigner rotation matrices of rank J. The subscripts of the Wigner functions are projection indices and denote components of the angular

momentum $\vec{J}$. The elements of the Wigner matrix are given according to eq. (69)

$$D^J_{m',m}(\alpha,\beta,\gamma) = \exp[-im'\alpha] d^J_{m',m}(\beta) \exp[-im\gamma] \tag{71}$$

where $d^J_{m',m}(\beta)$ are the corresponding reduced Wigner matrices.

We now summarize some basic properties of the Wigner matrices as follows:

1. Symmetry

$$D^{L^*}_{m',m}(\alpha,\beta,\gamma) = (-1)^{m'-m} D^L_{-m',-m}(\alpha,\beta,\gamma) = D^L_{m',m}(-\gamma,-\beta,-\alpha) \tag{72}$$

2. The product of two Wigner matrices of different ranks can be expressed in terms of the Clebsch-Gordan series.

$$\begin{aligned} D^{L_1}_{m'_1,m_1}(\Omega) D^{L_2}_{m'_2,m_2}(\Omega) &= \sum_{L,m,m'} C(L_1 L_2 L; m'_1 m'_2 m') \\ &\quad \times C(L_1 L_2 L; m_1 m_2 m) D^L_{m',m}(\Omega) \end{aligned} \tag{73}$$

where $C(L_1 L_2 L; m_1 m_2 m) \equiv C(L_1 L_2 L; m_1 m_2)$ denote the Clebsch-Gordan coefficients with $m = m_1 + m_2$.

3. The Wigner matrices are orthogonal due to

$$\begin{aligned} &\frac{1}{8\pi^2} \int_0^{2\pi} \int_0^{2\pi} \int_0^{\pi} D^{L_1 *}_{m'_1,m_1}(\alpha,\beta,\gamma) D^{L_2}_{m'_2,m_2}(\alpha,\beta,\gamma) d\alpha \sin\beta d\beta d\gamma \\ &\qquad = \frac{1}{2L_1+1} \delta_{m'_1 m'_2} \delta_{m_1 m_2} \delta_{L_1 L_2} \end{aligned} \tag{74}$$

4. Closure

$$\sum_n D^L_{m,n}(\alpha_1,\beta_1,\gamma_1)D^L_{n,m'}(\alpha_2,\beta_2,\gamma_2) = D^L_{m,m'}(\alpha,\beta,\gamma) \tag{75}$$

where the Euler angles (α,β,γ) are the resultant of two successive rotations by angles $(\alpha_1,\beta_1,\gamma_1)$ followed by angles $(\alpha_2,\beta_2,\gamma_2)$.

Finally, from properties 2 and 3 we find

$$\begin{aligned}\frac{1}{8\pi^2}\int_0^{2\pi}\int_0^{2\pi}\int_0^{\pi} D^{L_1}_{m_1',m_1}(\Omega)D^{L_2}_{m_2',m_2}(\Omega)D^{L_3*}_{m_3',m_3}(\Omega)d\Omega = \\ \frac{1}{2L_3+1}\delta_{m_1'+m_2',m_3'}\ \delta_{m_1+m_2,m_3} \\ \times C(L_1L_2L_3;m_1'm_2')C(L_1L_2L_3;m_1m_2)\end{aligned} \tag{76}$$

The Wigner rotation matrix elements are related to the modified (or normalized) spherical harmonics by

$$D^J_{m,0}(\alpha,\beta,\gamma) = C_{J,-m}(\beta,\alpha) = \sqrt{\frac{4\pi}{2J+1}}Y_{J,-m} \tag{77}$$

$$D^J_{0,m}(\alpha,\beta,\gamma) = C_{J,-m}(\beta,\gamma) \tag{78}$$

Appendix B

Diffusion Equation for Relaxation

B.1 Correlation Functions

In a stochastic Markovian process, the orientational correlation function for a uniaxial molecule can be written as

$$G^{LL'}_{mm'n}(t) = \int\int d\Omega_0 d\Omega P(\Omega_0) D^{L*}_{mn}(\Omega_0) \times P(\Omega_0|\Omega t) D^{L'}_{m'n}(\Omega) \tag{79}$$

where for simplicity, we use m and n to represent the m_L, the projection index in the laboratory frame and m_M, the projection index in the molecular frame, respectively. $\Omega \equiv (\alpha, \beta, \gamma)$ denotes the Euler angles, $P(\Omega_0|\Omega t)$ is the conditional probability of finding a molecule at orientation Ω at time t if the orientation of the molecule was Ω_0 at $t = 0$, and the equilibrium probability, $P(\Omega)$ is given by the Boltzmann distribution:

$$P(\Omega) = \frac{\exp[-U(\Omega)/kT]}{\int d\Omega \exp[-U(\Omega)/kT]} \tag{80}$$

where k is the Boltzmann constant and T is the temperature. $U(\Omega)$ is the potential of mean torque acting on the molecule [1], and its symmetry is determined by the symmetry of the molecule and that of the mesophase. For cylindrical molecules in the uniaxial phase, the potential of mean torque is governed by the β angle only, *i.e.* $U(\Omega) = U(\beta)$. For uniaxial molecules in biaxial mesophases (D_{2h} symmetry),

the potential of mean torque depends on two Euler angles, *i.e.* $U(\Omega) = U(\alpha, \beta)$ [2]. Now the effective anisotropic potential $U(\Omega)$ can be expanded in terms of Wigner matrices as

$$\frac{U(\alpha,\beta)}{kT} = \sum_{Jp} a_{Jp} D^{J}_{p0}(\alpha,\beta) \tag{81}$$

If the molecular reorientation takes place through a sequence of small angular steps, the evolution of the conditional probability $P(\Omega_0|\Omega t)$ can be described [3] by a differential equation for the diffusion process as

$$\frac{\partial P(\Omega_0|\Omega t)}{\partial t} = -\sum_{\alpha\beta} L_\alpha D_{\alpha\beta} \left[L_\beta + L_\beta \left(\frac{U(\Omega)}{kT} \right) \right] P(\Omega_0|\Omega t) \tag{82}$$

where $L_\beta = (L_x, L_y, L_z)$ is a component of a dimensionless angular momentum operator $\vec{L}$, and $\hat{D}$ is a rotational diffusion tensor. Here we take Nordio's model in which the diffusion tensor is diagonal in a molecular frame. For a symmetric top molecule we have $D_\perp$, the diffusion coefficient of the molecular z axis and $D_\parallel$, the diffusion coefficient around the molecular z axis as introduced in Chapter 2. The diffusion anisotropy parameter is defined as $\eta \equiv D_\parallel / D_\perp$. The above diffusion equation becomes

$$\begin{aligned} \frac{1}{D_\perp} \frac{\partial P(\Omega_0|\Omega t)}{\partial t} &= -\left[L_x^2 + L_x \left(L_x \frac{U(\Omega)}{kT} \right) \right] P(\Omega_0|\Omega t) \\ &\quad -\left[L_y^2 + L_y \left(L_y \frac{U(\Omega)}{kT} \right) \right] P(\Omega_0|\Omega t) \\ &\quad -\eta \left[L_z^2 + L_z \left(L_z \frac{U(\Omega)}{kT} \right) \right] P(\Omega_0|\Omega t) \\ &\equiv \vec{\Gamma} P(\Omega_0|\Omega t) \end{aligned} \tag{83}$$

where $\vec{\Gamma}$ is the diffusion operator which, for the purpose of numerical calculations,

can be rewritten using unitary transformation as

$$\begin{aligned}\hat{\Gamma} &= P^{-1/2}(\Omega)\vec{\Gamma}P^{1/2}(\Omega) \\ &= -\left[\nabla^2 + \frac{1}{2}\left(\nabla^2\frac{U(\Omega)}{kT}\right) - \frac{1}{4}\left(L_+\frac{U(\Omega)}{kT}\right)\left(L_+\frac{U(\Omega)}{kT}\right)\right. \\ &\quad \left. -\frac{1}{4}\eta\left(L_z\frac{U(\Omega)}{kT}\right)^2\right] \end{aligned} \tag{84}$$

where $P(\Omega)$ is given in eq. (80), the nobla operator $\nabla^2 = L_x^2 + L_y^2 + \eta L_z^2$ and $L_\pm = L_x \pm iL_y$ is the angular momentum step operator. The diffusion equation in this symmetrized form is given by

$$\frac{1}{D_\perp}\frac{\partial\hat{P}(\Omega_0|\Omega t)}{\partial t} = \hat{\Gamma}\hat{P}(\Omega_0|\Omega t) \tag{85}$$

where

$$\hat{P}(\Omega_0|\Omega t) = P^{-1/2}(\Omega)P(\Omega_0|\Omega t)P^{1/2}(\Omega_0) \tag{86}$$

is the symmetrized conditional probability. Now the symmetrized diffusion equation is easily solved using a matrix representation in a basis of normalized Wigner matrices [4] (see also Appendix A)

$$\mathcal{D}^L_{mn}(\Omega) = \sqrt{(2L+1)/8\pi^2}D^L_{mn}(\Omega) \tag{87}$$

In particular,

$$\hat{P}(\Omega_0|\Omega t) = \sum_{Lmn} C_{Lmn}(\Omega_0, t)\mathcal{D}^L_{mn}(\Omega) \tag{88}$$

where the expansion coefficients, C_{Lmn}, are evaluated by using the initial condition $\hat{P}(\Omega_0|\Omega 0) = \delta(\Omega - \Omega_0)$ to give

$$C_{Lmn}(\Omega_0, 0) = \mathcal{D}^{L*}_{mn}(\Omega_0) \tag{89}$$

By substituting Eq. (88) in Eq. (85), multiplying both sides on the left by $\mathcal{D}^{L*}_{mn}(\Omega)$ and integrating over Ω, a system of linear differential equations is obtained

$$\frac{1}{D_\perp}\dot{C}(t) = \hat{R}C(t) \tag{90}$$

$$\left(\hat{R}^n\right)_{L'm'Lm} = \int d\Omega \mathcal{D}^{L'*}_{m'n}(\Omega)\hat{\Gamma}\mathcal{D}^{L}_{mn}(\Omega) \tag{91}$$

In solving the above linear differential equations, a unitary eigenvector matrix $\hat{X}^n$ which diagonalizes the self-adjoint diffusion matrix $\hat{R}^n$ should be introduced

$$\hat{R}^n\hat{X}^n = \hat{X}^n\hat{r}^n \tag{92}$$

where $\hat{r}^n$ is a diagonal matrix that contains the eigenvalues of $\hat{R}^n$. The formal solution is

$$C^n(t) = \hat{X}^n \exp(tD_\perp \hat{r}^n)(\hat{X}^n)^T C^n(0) \tag{93}$$

Considering the matrix elements of $\hat{X}^n$ and substituting the zero time coefficients, we obtain

$$C_{Jpn}(\Omega_0, t) = \sum_K \sum_{J'p'} (\hat{X}^n)_{Jp,K} \exp(tD_\perp \hat{r}^n_K)(\hat{X}^n)^T_{J'p',K} \mathcal{D}^{J'*}_{p'n}(\Omega_0) \tag{94}$$

where K is used to label the eigenvalues of the diffusional matrix, $\hat{R}^n$. Using the un-normalized Wigner matrices here, the symmetrized conditional probability can be written as

$$\begin{aligned}\hat{P}(\Omega_0|\Omega t) = & \frac{1}{8\pi^2}\sum_{Kq}\sum_{Jp}\sum_{J'p'}\sqrt{2J+1}\sqrt{2J'+1} \\ & \times(\hat{X}^q)_{Jp,K}\exp(tD_\perp \hat{r}^q_K)(\hat{X}^q)_{J'p',K} \\ & \times D^J_{pq}(\Omega)D^{J'*}_{p'q}(\Omega_0)\end{aligned} \tag{95}$$

According to the asymptotic condition

$$\lim_{t\to\infty} P(\Omega_0|\Omega t) = P(\Omega) \tag{96}$$

All the exponentials in Eq. (95) decay to zero at infinite time except for the one corresponding to the zero eigenvalue, $\hat{r}_0^0$. The long time behavior of the symmetrized conditional probability, obtained as

$$\begin{aligned}
\lim_{t\to\infty} \hat{P}(\Omega_0|\Omega t) &= P^{1/2}(\Omega_0)P^{1/2}(\Omega) \\
&= \frac{1}{8\pi^2}\sum_{J''p''}\sum_{J'''p'''}\sqrt{2J''+1}\sqrt{2J'''+1} \\
&\quad \times(\hat{X}^0)_{J''p'',0}(\hat{X}^0)_{J'''p''',0}D^{J''}_{p''0}(\Omega)D^{J'''*}_{p'''0}(\Omega_0)
\end{aligned} \tag{97}$$

Substituting Eq. (95) and Eq. (97) to Eq. (79), the correlation functions can be expressed as

$$\begin{aligned}
G^{LL'}_{mm'n} &= \sum_K \exp(tD_\perp \hat{r}^n_K)\sum_{Jp}\sum_{J'p'}\sum_{J''J'''}\sqrt{\frac{(2J+1)(2J'+1)}{(2J''+1)(2J'''+1)}} \\
&\quad \times(\hat{X}^n)_{Jp,K}(\hat{X}^n)_{J'p',K}(\hat{X}^0)_{J'',m'-p;0}(\hat{X}^0)_{J''',m-p';0} \\
&\quad \times C(L,J',J''';m,-p')C(L,J',J''';n,-n) \\
&\quad \times C(L',J,J'';m',-p)C(L',J,J'';n,-n) \\
&= \sum_K (b^{LL'}_{mm'n})_K \exp[t(a^{LL'}_{mm'n})_K]
\end{aligned} \tag{98}$$

where $C(A,B,C;d,e)$ is the Clebsch-Gordan coefficient.

B.2 Spectral Densities

The spectral density $J^{(AB)}_{LL'mm'}(\omega)$ is given by a sum of Fourier-Laplace transfor-

mations of the correlation functions in Eq. (98)

$$J^{(AB)}_{LL'mm'}(\omega) = \sum_{nn'} A^{Ln*}_{MOL} B^{L'n'}_{MOL} \delta_{nn'} \int_0^\infty G^{LL'}_{mm'n}(t) \exp(-i\omega t) dt \tag{99}$$

where A^{Ln*}_{MOL} and $B^{L'n'}_{MOL}$ are single particle properties which are modulated by molecular reorientation. For deuteron NMR experiments, $L = L' = 2$. $A = B = \sqrt{3/2}\pi q_{CD} d^2_{n0}(\theta)$, where θ is the angle between the molecular z axis and the principal z axis of the efg tensor (*i.e.* the direction of C-D bond). The spectral densities for a uniaxial molecule in biaxial phases are given by

$$J_{mm'}(\omega) = \frac{3\pi^2}{2}(q_{CD})^2 \sum_n \left[d^2_{n0}(\theta)\right]^2 \sum_K \frac{(b^{22}_{mm'n})_K (a^{22}_{mm'n})_K}{(a^{22}_{mm'n})^2_K + \omega^2} \tag{100}$$

B.3 Calculations

In the calculations presented here, we investigate the simplest and most important case for the potential of mean torque, that is, only the second rank contribution to the potential of the mean torque is retained. Then

$$\frac{U(\alpha,\beta)}{kT} = a_{20}(T) P_2(\cos\beta) + a_{22}(T)[D^2_{20}(\alpha,\beta) + D^2_{-20}(\alpha,\beta)] \tag{101}$$

where $a_{2-2} = a_{22}$ was assumed [5]. Then the symmetrized diffusion operator given by Eq. (84) can be evaluated, which are

$$\begin{aligned}
\langle \mathcal{D}^{L'}_{m'n}| -\nabla^2 |\mathcal{D}^{L}_{mn}\rangle &= [-L(L+1) - n^2(\eta-1)]\delta_{L'L}\delta_{m'm} \\
\langle \mathcal{D}^{L'}_{m'n}| -\frac{1}{2}\nabla^2 \frac{U(\alpha,\beta)}{kT} |\mathcal{D}^{L}_{mn}\rangle &= -\frac{\sqrt{2L+1}}{2\sqrt{2L'+1}} \sum_{Jp} a_{Jp}[J(J+1)] \\
&\times\ C(L,J,L';m'-p,p) C(L,J,L';n,0)\delta_{m,m'-p}
\end{aligned}$$

$$
\begin{aligned}
& \langle \mathcal{D}^{L'}_{m'n} | \frac{1}{4} \left(L_+ \frac{U(\alpha,\beta)}{kT} \right) \left(L_- \frac{U(\alpha,\beta)}{kT} \right) | \mathcal{D}^{L}_{mn} \rangle \\
= & \frac{\sqrt{2L+1}}{4\sqrt{2L'+1}} \sum_{Jp} \sum_{J'p'} a_{JP} a_{J'p'} \sqrt{J(J+1)J'(J'+1)} \\
\times & \sum_{J''=|J-J'|}^{J+J'} C(J,J',J'';p,p') C(J,J',J'';1,-1) \\
\times & \; C(L,J'',L';m'-p-p',p+p') C(L,J'',L';n,0) \delta_{m,m'-p-p'} \qquad (102)
\end{aligned}
$$

In the above derivations, the following relations have been used:

$$
\nabla^2 \mathcal{D}^{L}_{mn} = [L(L+1) + (\eta - 1)n^2] \mathcal{D}^{L}_{mn} \qquad (103)
$$

$$
L_z \mathcal{D}^{L}_{mn} = n \mathcal{D}^{L}_{mn} \qquad (104)
$$

$$
L_\pm \mathcal{D}^{L}_{mn} = \sqrt{L(L+1) - n(n \pm 1)} \mathcal{D}^{L}_{mn} \qquad (105)
$$

Then, the matrix elements of $\hat{\Gamma}$ are given by

$$
\begin{aligned}
\langle \mathcal{D}^{L'}_{m'n} | \hat{\Gamma} | \mathcal{D}^{L}_{mn} \rangle &= (\hat{R}^n)_{L'm'Lm} \\
&= [-L(L+1) - n^2(\eta - 1) + K_0] \delta_{LL'} \delta_{m'm} \\
&+ \frac{\sqrt{2L+1}}{\sqrt{2L'+1}} K_1 C(L,2,L';m',0) C(L,2,L';n,0) \delta_{m'm} \\
&+ \frac{\sqrt{2L+1}}{\sqrt{2L'+1}} K_2 [C(L,2,L';m'-2,2) \delta_{m,m'-2} \\
&+ C(L,2,L';m'+2,-2) \delta_{m,m'+2}] C(L,2,L';n,0) \\
&+ \frac{\sqrt{2L+1}}{\sqrt{2L'+1}} K_3 C(L,4,L';m',0) C(L,4,L';n,0) \delta_{m'm} \\
&+ \frac{\sqrt{2L+1}}{\sqrt{2L'+1}} K_4 [C(L,4,L';m'-2,2) \delta_{m,m'-2} \\
&+ C(L,4,L';m'+2,-2) \delta_{m,m'+2}] C(L,4,L';n,0)
\end{aligned}
$$

$$+ \quad \frac{\sqrt{2L+1}}{\sqrt{2L'+1}} K_5 [C(L,4,L';m'-4,4)\delta_{m,m'-4}$$

$$+ \quad C(L,4,L';m'+4,-4)\delta_{m,m'+4}]C(L,4,L';n,0) \qquad (106)$$

The following constants have been used in the above equation

$$\begin{aligned} K_0 &= -\frac{3}{5}(\frac{1}{2}a_{20}^2 + a_{22}^2) \\ K_1 &= -3a_{20} - \frac{3}{7}(\frac{1}{2}a_{20}^2 - a_{22}^2) \\ K_2 &= -3a_{22} + \frac{3}{7}a_{20}a_{22} \\ K_3 &= \frac{6}{35}(3a_{20}^2 + a_{22}^2) \\ K_4 &= \frac{6}{7}\sqrt{\frac{3}{5}}a_{20}a_{22} \\ K_6 &= 3\sqrt{\frac{2}{35}}a_{22}^2 \end{aligned} \qquad (107)$$

For uniaxial phases, $L = L' = 2$ for deuteron and $a_{22} \equiv 0$ which makes $K_2 = K_4 = K_5 = 0$. The matrix elements of $\hat{\Gamma}$ are identical to zero unless $m' = m$. In this limit case, we replace the projection indices m, n and K by m_L, m_M and j, respectively and rewrite the eq. (98) as follows

$$G^2_{m_L m_M} = \sum_j (b^2_{m_L m_M})_j \exp[t(a^2_{m_L m_M})_j] \qquad (108)$$

Comparing the above equation with Eq. (37) in Chapter 2, It is realized that this is just the expression of Volds' numerical results.

Reference

1. G.R. Luckhurst, The Molecular Physics of Liquid Crystals, edited by G.R. Luckhurst and G.W. Gray, Academic, New York, 1979, Chap. 4, p.85.

2. C.Zannoni and M. Guerra, Mole. Phys. 44, 849, 1981.

3. P.L. Nordio and U. Segre, The Molecular Physics of Liquid Crystals, edited by G.R. Luckhurst and G.W. Gray, Academic, New York, 1979, Chap. 18, p.411.

4. R. Tarroni and C. Zannoni, J. Chem. Phys. 95, 4550, 1991.

5. F. Biscarini, C. Chiccoli, P. Pasini, F. Semeria, and C. Zannoni, 14th International Liquid Crystal Conference, 1992.

6. E. Berggren, R. Tarroni, and C. Zannoni, J. Chem. Phys. 99, 6180, 1993.